An atypical ABC transporter is involved in antifungal resistance and host interactions in the pathogenic fungus *Cryptococcus neoformans*

Christopher J. Winski[a], Yuanyuan Qian[b], Shahriar Mobashery[b], Felipe H. Santiago-Tirado[a#]

[a]Department of Biological Sciences, [b]Department of Chemistry and Biochemistry, University of Notre Dame, Notre Dame, Indiana, 46656, USA

Running Head: A PDR transporter with dual roles in *C. neoformans*

#Address correspondence to Felipe H. Santiago-Tirado, fsantiag@nd.edu

Word Counts

Abstract: 240

Importance: 147

Text: 6098

ABSTRACT

ATP-binding cassette (ABC) transporters represent one of the largest protein superfamilies. Functionally diverse, ABC transporters have been implicated in many aspects of microbial physiology. The genome of the human fungal pathogen *Cryptococcus neoformans* encodes 54 putative ABC transporters and the majority of them remain uncharacterized. In a previous genetic screen for fungal regulators of phagocytosis, we identified an uncharacterized gene, CNAG_06909, that modulates host interactions. This gene encodes a half-size ABC transporter of the PDR-type, and phenotypic studies of a strain missing this gene revealed an altered antifungal profile, including hypersensitivity to fluconazole (FLC). This gene, which we have named *PDR6*, localizes to the endoplasmic reticulum (ER) and plasma membrane (PM), and when absent, less ergosterol was observed in the PM. Additionally, we observed that the *pdr6*Δ strain displays a reduction in secreted polysaccharide capsular material. These changes to the cellular surface may explain the observed increased uptake by macrophages and the reduced intracellular survival. Finally, studies in mice demonstrate that *PDR6* function is required for normal progression of cryptococcal infection. Taken together, this study demonstrates a novel dual role for PDR transporters in *C. neoformans*, which could represent a potential target for antifungal therapeutics. Furthermore, the atypical half-size transporter encoded by *PDR6* is conserved in many fungal pathogens, but absent in non-pathogenic fungal models. Hence, this study provides for the first time, a function for this unique group of fungal half-size PDR transporters that, although conserved, remain largely understudied.

IMPORTANCE

Conserved across all kingdoms of life, ABC transporters comprise one of the largest protein families. They are associated with multidrug resistance, affecting aspects such as resistance to antimicrobials or cancer treatments. Despite their importance, they are understudied in fungal pathogens. In the environmental fungus *Cryptococcus neoformans*, a leading cause of fungal infections, only few ABC transporters have

been studied. Here we characterize an atypical, half-size, ABC transporter of the PDR-type, that affects both antifungal resistance and host-pathogen interactions. PDR-type transporters are only present in fungi and plants, and this subgroup of half-size transporters is conserved in fungal pathogens, yet their function was completely unknown. Because the current treatments for cryptococcal infection are suboptimal, understanding the mechanisms of antifungal resistance and the host interactions that drive the infection is critical to improve the management of this disease. Here we provide insights into these important aspects of cryptococcal pathogenesis.

INTRODUCTION

Present in every living organism, ATP-binding cassette (ABC) transporters constitute a large superfamily of integral membrane proteins. Functionally, ABC transporters are responsible for the transport of diverse substrates across membranes, but have also been implicated in mRNA translation and peroxisome biogenesis (1, 2). Structurally, ABC transporters contain at least one nucleotide-binding domain (NBD) and one transmembrane domain (TMD), both of which are evolutionary conserved. Most ABC transporters have a domain arrangement of TMD1-NBD1-TMD2-NBD2 ($[TMD\text{-}NBD]_2$) (3). The orientation and molecular architecture of these domains is used to organize ABC transporters into subgroups. The pleiotropic drug resistance (PDR) subgroup, which is present in only fungi and plants, has a reverse configuration $[NBD\text{-}TBD]_2$ (4, 5). Identified and predominantly studied in the non-pathogenic yeast *Saccharomyces cerevisiae*, they remain understudied in pathogenic fungi. This is despite the abundance of fungal PDR proteins and the fact that fungal infections globally kill close to 1.6 million people yearly (6, 7). The few that have been studied mostly act as efflux pumps for xenobiotics or antifungal drugs. Nonetheless, the sheer number and diversity of PDR genes found in fungal genomes suggests a broad involvement in cellular processes. Moreover, there is a subgroup of half-size PDR transporters (containing only one NBD and TMD) whose function remains unknown.

71 *Cryptococcus neoformans* is an environmental, opportunistic fungal pathogen responsible for
72 over 180,000 deaths annually in the HIV+ population alone (8, 9). Upon inhalation and subsequent lung
73 colonization, *C. neoformans* can disseminate to the central nervous system (CNS) resulting in cryptococcal
74 meningitis, with a mortality rate as high as 81% (9). The high mortality rate is a direct consequence of the
75 complexities associated with cryptococcal pathogenesis coupled with a paucity of effective antifungals.
76 Currently, the most effective treatment for cryptococcal meningitis includes a combinatorial regimen of
77 amphotericin B (AMB) and 5-flucytosine (5-FC). AMB is a fungicidal polyene that targets ergosterol, an
78 essential lipid in the fungal plasma membrane. The pyrimidine 5-FC disrupts DNA/RNA synthesis (10).
79 Notwithstanding toxicity associated with these agents, they are also costly, which makes them less
80 available to resource-poor countries, where the need is highest. Instead, patients in these regions are
81 treated with the less effective fluconazole (FLC) monotherapy. FLC is a fungistatic azole that inhibits
82 lanosterol 14α-demethylase, an enzyme in the ergosterol biosynthesis pathway encoded by *ERG11* (11).
83 FLC monotherapy has not only been implicated in higher relapse rates, but several recent studies have
84 reported an increase in the incidence of FLC resistance in *C. neoformans*, making the treatment of
85 cryptococcal meningitis even more challenging (12, 13).

86 Several FLC resistance mechanisms have been reported in *C. neoformans*. These vary from
87 mutations in the *ERG11* gene to heteroresistance due to genome plasticity including polyploidy,
88 aneuploidy, loss of heterozygosity, and copy-number variation (14-17). Additionally, the overexpression
89 of ABC efflux pumps has been implicated in FLC resistance (18). There are 54 putative ABC transporters in
90 the *C. neoformans* genome and only a few have been characterized. The roles of *C. neoformans AFR1*,
91 *AFR2*, and *MDR1* as azole efflux pumps have been well documented, where *AFR1* functions as the major
92 pump and *AFR2* and *MDR1* provide additive roles in the management of FLC stress (19-21). It is evident
93 that the function of most of the ABC transporters encoded in the *C. neoformans* genome remain unknown.
94 In an earlier report on fungal regulators of phagocytosis, we identified an uncharacterized gene,

95 CNAG_06909, as a modulator of the fungal-host interaction (22). In the present study, we demonstrate
96 that CNAG_06909 encodes a half-size PDR-transporter and that disruption of the gene results in
97 hypersensitivity to FLC. We have designated the gene as pleiotropic drug resistance-6 (*PDR6*) because it
98 does not have a direct ortholog in the model yeast, *S. cerevisiae* and the molecular architecture is
99 consistent with the PDR subgroup of ABC transporters. We show that Pdr6 does not function as a FLC
100 efflux pump but its deletion results in decreased levels of ergosterol in the PM, accompanied by mild
101 thermosensitivity and decreased secretion of capsular material. These phenotypes are unique to *PDR6* as
102 they were not observed in the previously characterized ABC transporters. Furthermore, the *pdr6*Δ strain
103 exhibits diminished intracellular survival *in vitro* and is attenuated in a murine model of infection. When
104 the gene is expressed in a model yeast, it localizes to the ER and PM, consistent with a role in ergosterol
105 synthesis/transport. Notably, this study provides for the first time a function for an atypical conserved
106 half-size PDR transporter, which has remained largely obscure. These studies highlight the importance of
107 fungal PDR-type transporters and broaden our understanding of the specialization of ABC transporters in
108 microbial pathogens.
109

110 **RESULTS**

111 ***C. neoformans PDR6* is a member of a conserved group of half-size PDR transporters**

112 Present in only fungi and plants, PDR-type ABC transporters represent a unique subset of proteins
113 primarily implicated in drug resistance and detoxification (4). Although fungal PDR-type transporters
114 closely resemble mammalian ABCG transporters, which are half-size, only the full-size fungal PDR proteins
115 have been analyzed and studied (23, 24). Given that *C. neoformans PDR6* is half-size, we performed a
116 phylogenetic analysis to determine how widespread *PDR6* sequences are in the fungal kingdom (Fig. 1A).
117 All fungi belonging to the Pezizomycotina subphylum and pathogenic fungi subphyla have a *PDR6*
118 ortholog, implicating *PDR6* in fungal pathogenesis in many subphyla. Regardless of the presence of a *PDR6*

119 ortholog, all the PDR-type ABC transporter genes in Figure 1A were used to construct a global phylogenetic
120 tree (Fig. 1B). Analysis of the fungal PDR genes showed the presence of seven major clades. Clade I is the
121 largest and includes *S. cerevisiae PDR5*, *PDR10*, *PDR15*, and *C. neoformans AFR2*. Clade II is the smallest
122 and contains sequences that are homologous to *S. cerevisiae PDR12*, *PDR18* and *SNQ2.* Clade III sequences
123 are absent in Saccharomycotina, but contain *C. neoformans AFR1*. *S. cerevisiae PDR11* and *AUS1*
124 represent the genes in clade IV. Clades I, II, III, IV, and VIa all contain full-length *PDR* genes, whereas clades
125 V and VIb represent atypical groups of PDR genes that only encode one nucleotide-binding domain (NBD)
126 and one transmembrane domain (TMD). *S. cerevisiae ADP1* is representative of the genes in clade V that
127 all contain a NBD and TMD with an additional unique sequence (most commonly an EGF domain). *C.*
128 *neoformans PDR6* and the eleven other half-size PDR genes in clade VIb represent a completely
129 uncharacterized group of fungal genes with no known function. Interestingly, the fungi represented in
130 clade VIb are all plant or animal pathogens, again suggestive that *PDR6* and its orthologs may be
131 implicated in fungal virulence. Topology prediction by CAMPS shows that *C. neoformans PDR6* encodes a
132 626 amino acid half-size transporter, with a single NBD containing characteristic Walker A and ABC motif
133 features followed by a single TMD, composed of six transmembrane helices (Fig. 1C). These analyses show
134 that *C. neoformans PDR6* encodes a half-size PDR-type ABC transporter that is evolutionarily conserved,
135 present in all fungal pathogens that we analyzed, and contains all the features of a functional full-length
136 ABC transporter.
137
138 **Deletion of *PDR6* affects resistance to azoles and the drug profile of other antifungals**
139 Given that cryptococcal PDR-type ABC transporters Afr1 and Afr2 have been implicated in the efflux and
140 resistance of antifungal compounds (20, 21), we hypothesized that Pdr6 would function in a similar
141 manner. To assess the function/specificity of Pdr6, we used a *C. neoformans* strain lacking the *PDR6* gene
142 (*pdr6*Δ) and tested its growth on FLC gradient plates and Etest strips (Fig. 2A) and performed broth

143 microdilution assays to measure the minimal-inhibitory concentrations (MICs) of several related
144 compounds (Fig. 2B-G and Table 1). Compounds included five azole-class antifungals (fluconazole (FLC),
145 itraconazole (ITC), voriconazole (VRC), ketoconazole (KTC), and posaconazole (PSC)), one polyene-class
146 antifungal (amphotericin B (AMB)), one DNA/RNA synthesis inhibitor (5-fluorocytosine (5-FC)), one
147 protein-synthesis inhibitor (cycloheximide (CHX)), one antineoplastic agent (nocodazole), two other
148 xenobiotics (berberine (BER), and paraquat (PQ)), one superoxide generator (menadione), and one
149 echinocandin-class antifungal (caspofungin (CSF)). In addition to the *pdr6*Δ mutant strain, we used the
150 *afr1*Δ, *afr1*Δ/*afr2*Δ/*mdr1*Δ, and *erg3*Δ strains as controls, since all have displayed increased FLC
151 susceptibility (21, 25).

152 Among the compounds tested, we found that the *pdr6*Δ mutant displayed a hypersensitive
153 phenotype specifically towards the azole class antifungals, albeit not as drastic as the *afr1*Δ,
154 *afr1*Δ/*afr2*Δ/*mdr1*Δ, or *erg3*Δ strains (Fig. 2 and Table 1). The MICs of the non-azole compounds in the
155 *pdr6*Δ strain were comparable to those of the H99 WT, suggesting a specific role of Pdr6 in fluconazole
156 resistance. Additionally, previous studies have shown a relationship between environmental pH and
157 antifungal efficacy (26), so we performed similar assays at alkaline and acidic conditions (Fig S1).
158 Regardless of the pH, the MICs of the WT and *pdr6*Δ strains displayed similar trends suggesting that *PDR6*
159 functions in a pH-independent manner.

160 Given the increase in azole susceptibility by the *pdr6*Δ mutant, we performed checkerboard assays
161 with four common antifungals, FLC, AMB, 5-FC, and CSF (Fig. 3). Interestingly, we found that FLC coupled
162 with CSF functions differently in the *pdr6*Δ strain when compared to the WT. The combination works in a
163 synergistic manner in the *pdr6*Δ strain and only in an additive manner in the WT. This finding was
164 unexpected given that CSF is ineffective at treating cryptococcal infections. Additional experimentation is
165 required to explain the observed finding. Nonetheless, these data show that *PDR6* is involved in azole

166 resistance, is not affected by pH, and can alter antifungal combinatorial behaviors. All of these results
167 were confirmed using three independently recreated *pdr6*Δ mutants (Fig. S2 and Materials and Methods).
168

169 **Deletion of *PDR6* does not affect drug accumulation**

170 The increased azole susceptibility of the *pdr6*Δ mutant led us to hypothesize that Pdr6 could function as
171 an efflux pump, similar to many of the characterized fungal PDR transporters. Rhodamine 6G (R6G) and
172 Nile Red (NR) are fluorescent xenobiotics that have been used as generic probes to measure ABC
173 transporters' efflux activity (27, 28). To determine if Pdr6 functions as an efflux pump, we measured the
174 intracellular accumulation of R6G and NR by flow cytometry (Fig. 4A). Surprisingly, no difference was
175 observed in the mean fluorescent intensity (MFI) values of either R6G or NR in the *pdr6*Δ mutant,
176 compared to the WT. In contrast, the *afr1*Δ and *afr1*Δ/*afr2*Δ/*mdr1*Δ strains accumulated high levels of
177 these xenobiotics. We reasoned that Pdr6 may not recognize R6G or NR and potentially, Pdr6 is strictly an
178 azole-specific transporter. To test this, we synthesized a dansyl amide labeled-FLC molecule, termed
179 Probe 1 (Fig. 4B), that has been used to visualize the intracellular localization of FLC in *Candida albicans*
180 (29). Although the modification of FLC with dansyl amide affected its antifungal activity, the strains
181 sensitive to FLC were also sensitive to Probe 1, indicating a similar mechanism of action (Fig. 4B).
182 Consistently, the intracellular accumulation of Probe 1 was significantly increased in the *afr1*Δ and
183 *afr1*Δ/*afr2*Δ/*mdr1*Δ strains (Fig. 4C). However, there was no difference in the intracellular accumulation
184 of Probe 1 between the *pdr6*Δ strain and WT, suggesting that Pdr6 is not a major efflux pump for FLC and
185 instead affects azole activity by a different mechanism. We also used light microscopy to assess the
186 intracellular localization and accumulation/fluorescent intensity of Probe 1 between strains and no
187 differences in location were observed, while fluorescent intensity values supported the findings above
188 (data not shown). To provide definitive support that Pdr6 is not acting as a FLC-specific efflux pump, we
189 directly measured accumulation of FLC using a liquid chromatography-mass spectrometry (LC-MS)-based

190 FLC accumulation assay (Fig. 4D). We found that the *pdr6*Δ mutant once again displayed levels comparable
191 to the WT, while the *afr1*Δ/*afr2*Δ/*mdr1*Δ positive control strain accumulated significant amounts of FLC.
192 Taken together, these data support that Pdr6 is not functioning as a drug-efflux pump and that the
193 hypersensitivity to azole antifungals in the *pdr6*Δ strain is not due to increased accumulation of these
194 drugs.
195
196 ***PDR6* is involved in ergosterol trafficking**
197 To mechanistically explain Pdr6's contribution to antifungal resistance, we next considered azoles' mode
198 of action. It is well documented that the target of azoles is Erg11, an enzyme in the ergosterol biosynthesis
199 pathway (15, 30). Disruptions to the ergosterol metabolic pathway can result in accumulation of sterols,
200 which have been implicated in both diminished and increased effectiveness of azole compounds (25, 31).
201 We, therefore, hypothesized that the azole resistance phenotype might be a result of *PDR6*'s involvement
202 in ergosterol transport. To quantify ergosterol content in the cryptococcal plasma membrane, we used
203 filipin, a sterol-binding fluorescent dye (Fig. 5A). We found a significant difference in fluorescence
204 between the WT and the *pdr6*Δ mutant. Specifically, the deletion of *PDR6* resulted in decreased
205 fluorescence, suggesting that less sterol is present and that Pdr6 plays a role in either the synthesis of
206 sterols or their trafficking; ABC transporters have been implicated in the latter (1, 32, 33), supporting a
207 potential role for Pdr6 in ergosterol transport to the plasma membrane. The quantitative microscopy
208 results were further supported using a fluorescent plate reader, which confirmed that the *pdr6*Δ mutant
209 has reduced overall ergosterol, compared to the WT (Fig. 5B). These findings provide context for the
210 previously observed antifungal phenotype and demonstrate that the *pdr6*Δ strain has an altered plasma
211 membrane with less ergosterol, consistent with a role of *PDR6* in ergosterol transport/trafficking. Lastly,
212 an indirect role of *PDR6* in azole resistance is supported by the fact that the presence of FLC does not
213 affect the expression of *PDR6*, while growth under host-like conditions induce a rapid and sustained

214 increase in transcript levels (Fig. S3). Ergosterol is essential for thermotolerance and survival inside
215 mammalian hosts (33), so if *PDR6* is involved in ergosterol transport, then it would be expected to be
216 overexpressed under host-like conditions.
217
218 **Pdr6 localizes to the ER and plasma membrane**
219 To better understand the function of Pdr6, we generated a C-terminally tagged Pdr6-GFP integrative
220 construct under the control of the *PDR5* promoter and introduced it into the *S. cerevisiae* strain ADΔΔ (34,
221 35). This strain is missing seven major endogenous ABC transporters and expresses a mutant Pdr1
222 transcription factor, driving overexpression of PDR genes. This strain not only allows for the visualization
223 of Pdr6 localization, but also a more direct assessment of efflux activity, provided cryptococcal Pdr6 would
224 be the only major PDR protein in the cell. Visualization of the ADΔΔ+Pdr6-GFP strain revealed clear
225 perinuclear and peripheral staining, characteristic of the yeast endoplasmic reticulum (ER) (Fig. 6A).
226 Images also revealed small areas of intense localization or puncta that were present in the ER and/or
227 plasma membrane as determined through Z stacks (Fig. 6A and S4A). Similarly, a control ADΔΔ strain
228 expressing Afr1-GFP, a full-length PDR-type transporter, displayed similar localization patterns in the ER
229 and plasma membrane, although lacking the puncta present in the ADΔΔ+Pdr6-GFP strain (Fig. 6A and
230 S4B). Using the same set of strains, we measured FLC susceptibility with Etest strips. The strain expressing
231 Afr1-GFP, a known FLC efflux pump, exhibited an 12-fold increase in MIC (MIC = 0.75 μg/mL) over the
232 ADΔΔ+empty vector (MIC = 0.064 μg/mL) control (Fig. 6B). In contrast, the ADΔΔ+Pdr6-GFP strain
233 exhibited a modest increase with a MIC of 0.25 μg/mL, resulting in a 4-fold increase over the control but
234 a 3-fold decrease compared to the ADΔΔ+Afr1-GFP strain. This small increase in MIC could be due to the
235 potential role of Pdr6 in ergosterol transport. To test this, we subjected the set of ADΔΔ strains to filipin
236 staining and analysis as above. Consistently, the ADΔΔ strains with an empty vector or expressing Afr1-
237 GFP had the lowest plasma membrane fluorescence, while the ADΔΔ+Pdr6-GFP had intermediate

238 fluorescence, and the wild-type background control had the highest fluorescence (Fig. 6C). Since the ER is
239 the site of fungal sterol synthesis, taken together, these results suggest that the role of Pdr6 in azole
240 resistance stems from effects on ergosterol synthesis and/or transport and not from acting as a specific
241 FLC efflux pump.
242
243 ***PDR6* influences interaction with host macrophages**
244 Alveolar macrophages represent the first line of defense against cryptococcal infections and the complex
245 fungal-phagocyte interaction ultimately determines the course of infection and patient outcome (36). We
246 initially identified *PDR6* in a screen for fungal regulators of phagocytosis (22). We used the same
247 automated high-content imaging method to quantify the phagocytic index (PI) of the library's *pdr6*Δ strain
248 and the recreated strains by a human monocytic cell line (THP-1) (Fig. 7A and S2B). In agreement, the
249 original and recreated *pdr6*Δ mutants were all phagocytosed more readily than the WT, providing
250 evidence that changes in phagocytosis are a direct result of loss of *PDR6* function. The *pka1*Δ strain served
251 as a high-uptake positive control. This observation begs the question of how the deletion of an atypical
252 PDR-type ABC transporter was affecting the cryptococcal-host interaction. We first tested if the absence
253 of *PDR6* affected the cryptococcal capsule. The *pdr6*Δ mutant was able to generate capsule comparable
254 to the WT, indicating that *PDR6* is not involved in capsule formation (Fig. S5A). Next, we assessed if there
255 were any defects in cell-wall structure by growing *pdr6Δ*, WT, *afr1*Δ, and *afr1*Δ/*afr2*Δ/*mdr1*Δ strains under
256 cell-wall-stress conditions (Fig. S5B). All strains grew under the tested conditions, and melanized normally,
257 suggesting that there are no defects in the cell wall (Fig. S5B, C). Finally, we hypothesized that *PDR6* was
258 involved in the secretion/efflux of an immunomodulatory factor and thus influencing host interactions.
259 To test this idea, we performed similar uptake assays as previously described, but used strain-specific
260 conditioned media (CM) during the cryptococcal-macrophage coincubation. The thought process being
261 that if *PDR6* is in fact responsible for the release of an immunomodulatory compound, then the CM from

262 the *pdr6*Δ strain should influence the uptake of the WT as to increase the PI values, whereas the CM from
263 the WT should decrease the PI values of the *pdr6*Δ strain. As shown in Fig. 7B, there were significant
264 differences in phagocytosis dependent on the source of the CM. Specifically, the incubation of the WT
265 with *pdr6*Δ CM increased uptake 2-fold, while the incubation of the *pdr6*Δ strain with WT CM significantly
266 decreased uptake back to WT levels. Notably, use of CM from the *afr1*Δ mutant had no significant impact
267 on the PI values of either WT or *pdr6*Δ strains. This suggests that *PDR6* is involved in the release of an
268 immunomodulatory factor that is present in the media and significantly impacts phagocytosis of
269 cryptococcal cells by host phagocytes. Taken together, these data confirm that the *pdr6*Δ mutant is
270 recognized and phagocytosed more avidly than the WT strain, and that the deletion of *PDR6* alters the
271 secretion/efflux of fungal immunomodulatory compounds.
272
273 ***PDR6* is involved in capsular shedding and adherence**
274 To investigate in more detail how *PDR6* is altering the cryptococcal-phagocyte interaction, we focused on
275 the polysaccharide capsule. Primarily composed of glucuronoxylomannan (GXM) and
276 glucuronoxylomannogalactan (GXMGal), the capsule is known to be secreted/shed in a constitutive
277 manner. This secreted capsule plays a central role in virulence by acting as an antiphagocytic factor,
278 providing protection against host stressors, and modulating the host immune response (37, 38). We
279 wondered if the release/secretion of the capsule into the surrounding environment is altered in the *pdr6*Δ
280 mutant. To test this, we analyzed the amount of shed capsule by electrophoresis and immunoblotting
281 using anti-GXM antibodies (Fig. 8A) (39). Quantification of the immunoblot showed that the *pdr6*Δ mutant
282 sheds significantly less capsule compared to the WT in both DMEM and YNB media (Fig. 8A). Notably,
283 there were no differences in shed capsule between the *afr1*Δ and *afr1*Δ/*afr2*Δ/*mdr1*Δ strains and the WT,
284 indicating that this phenotype is unique to the Pdr6 transporter. As expected, there was no GXM secreted
285 from the *cap59*Δ strain. This observed defect in capsule shedding could explain the phagocytosis

286 phenotype, but to further test if there are functional consequences associated with this defect, we
287 performed biofilm/adherence assays (Fig. 8B). Previous studies have shown that GXM is essential for the
288 formation of cryptococcal biofilms (40-42). Consistently, we found a similar trend where the *pdr6*Δ strain
289 formed weaker/less biofilm structures when compared to the WT, as measured by biomass quantification
290 using anti-GXM antibody. Identical results were obtained by metabolic quantification using XTT reduction
291 assays (data not shown). Taken together, these data suggest that *PDR6* is implicated in the shedding of
292 the polysaccharide capsule, affecting both phagocytosis by host cells and biofilm formation.
293

294 ***PDR6* function is required for *in vitro* and *in vivo* virulence**

295 Given the altered host interactions exhibited by the *pdr6*Δ mutant, its mild thermotolerance (Fig. S5D),
296 and the decreased capsule shedding, we next assessed its ability to survive within the challenging and
297 harsh intracellular environment. To test this, we performed *in vitro* survival assays and found that the
298 *pdr6*Δ mutant struggled to survive within host macrophages when compared to the WT (Fig. 9A). After 4h
299 in the presence of naïve human macrophages, ~10% of intracellular WT cells died, whereas ~40% of the
300 *pdr6*Δ cells are killed. To expand on this mild *in vitro* defect, we tested the virulence of the *pdr6*Δ mutant
301 in a murine inhalation model of cryptococcosis, monitoring disease progression by weight loss. Infection
302 with the WT strain resulted in all animals steadily losing weight by about two weeks, 50% of them dying
303 in 17 days, and all succumbing to infection by day 19 (Fig. 9B). In contrast, mice infected with the original
304 *pdr6*Δ and the recreated *pdr6*Δ-1 strains lived about two weeks longer than the WT-infected mice, with
305 animals beginning to die at day 34, and all succumbing to infection by day 41, thus showing a significant
306 increase in survival. Notably, CFUs recovered from these mice at time of death showed similar lung burden
307 as WT, but significantly less dissemination to brain and spleen (Fig. 9C), supporting an altered progression
308 or attenuated pathology. Consistently, the *pdr6*Δ-infected mice exhibited respiratory symptoms (rapid
309 and labored breathing), and their lungs were significantly more inflamed and enlarged than the WT lungs

310 at time of death. Taken together, these data suggest that *PDR6* function is required for full cryptococcal
311 pathogenesis, and in its absence, the manifestation of the disease is more consistent with pneumonia
312 rather than typical meningitis.
313

314 **DISCUSSION**

315 The H99 genome contains 10 genes encoding PDR-type ABC transporters. Although it has a conserved
316 representative gene in all clades except clade II, few have been characterized. Here we present an initial
317 characterization of an atypical, half-size, PDR transporter found in a fungal-host interaction screen. This
318 gene, which we call *PDR6*, is conserved in the fungal kingdom (clade VIb), but no function has been
319 reported for that subgroup. Since all the other members of that clade are pathogenic fungi, our work may
320 have broad implication for medically-important fungi. Given the similarity of *PDR6* to *AFR1* and *AFR2*,
321 which have been shown to act as efflux pumps for FLC, we tested the hypothesis that *PDR6* might act in a
322 similar way. However, our data shows that it is unlikely that Pdr6 is an efflux pump for the compounds
323 tested, including FLC. The *pdr6*Δ mutant accumulates the same level of all these compounds, yet it is
324 hypersensitive to them.

325 We then focused on ergosterol, the direct or indirect target of most antifungal drugs. Studies in
326 the model yeast *S. cerevisiae* have documented the ergosterol biosynthetic pathway in detail (43). This
327 occurs in the ER, yet how ergosterol is trafficked to the plasma membrane is not known, although it is
328 known that it does not involve vesicular traffic (44). In this yeast, *PDR18* has been implicated in that
329 process, and indeed, when *PDR6* is compared to the *S. cerevisiae* genome, *PDR18* is the gene closest to it,
330 although there is no real *PDR6* homolog in *S. cerevisiae*. Moreover, fungal and plant PDR genes are part
331 of the subfamily G of ABC transporters. In mammals, all ABCG members are half-size, and the mouse
332 ABCG3 and human ABCG5 and 8 transporters are all involved in cholesterol transport (45). Interestingly,
333 a BLAST analysis of these ABCG sequences against the *Cryptococcus* genome identifies *PDR6* as the gene

334 with the highest similarity to ABCG3 and 8. Hence, our finding that Pdr6-GFP localizes to the ER and to the
335 PM, the biosynthesis site and final destination of ergosterol, respectively, and that the *pdr6*Δ mutant has
336 decreased ergosterol while the ADΔΔ+Pdr6-GFP increases plasma membrane ergosterol, strongly support
337 a model were Pdr6 functions as an ergosterol transporter.

338 It is known that defects in the plasma membrane can affect the cell wall and/or capsule. We did
339 not find evidence for gross alterations to either of these layers, but the defect in capsule shedding, and
340 the results of the CM studies, are highly suggestive of Pdr6 having a role in regulated shedding of the
341 capsule. It has been shown that capsule is shed constitutively, but recent studies have demonstrated that
342 capsule shedding can also be regulated (38). *PDR6* is highly and rapidly induced under host conditions,
343 which are conditions known to induce capsule growth and shedding. Notably, it is known that normal
344 levels of ergosterol are needed for thermotolerance, hence if *PDR6* is involved in ergosterol homeostasis,
345 it would be expected to be induced upon shift to body temperature. The altered ergosterol levels in the
346 *pdr6*Δ mutant could explain both the increased sensitivity to FLC and other azoles, and the mild
347 thermotolerance (Fig. 10).

348 Lastly, we show that Pdr6 function is needed for normal progression and disease manifestation in
349 the mouse inhalational model. This could be explained by the decreased capsular shedding, high
350 phagocytosis, and lower intracellular survival (Fig. 10). The increased recognition and phagocytosis could
351 give the host an advantage since the fungus does not survive as well intracellularly. This would affect
352 dissemination, as there is ample evidence that phagocytes are needed for extrapulmonary dissemination,
353 a process known as trojan-horse transit (46). However, in order for trojan-horse transit to occur, the
354 fungus must be able to survive intracellularly, and the *pdr6*Δ mutant is defective in this respect. Moreover,
355 the decreased capsule shedding from the extracellular fungi would result in a stronger inflammatory
356 response. The *pdr6*Δ mutant is also capable of inducing production of a large capsule, hence over time,
357 less cells would be phagocytosed, and free cells in the tissue would accumulate. With the increased fungal

358 burden, and the stronger inflammatory response, the host advantage is lost, and the animals die exhibiting
359 different symptoms. Ongoing studies into the immunological response of the animals to *pdr6*Δ infection
360 will shed more light into this hypothesis.

361 In conclusion, we have described a new mechanism by which cryptococcal cells can modulate
362 their susceptibility to azoles: ergosterol transport regulated by Pdr6. Our results with the CM also indicate
363 a potential new antiphagocytic mechanism: the *pdr6*Δ mutant can still grow a capsule, yet it is recognized
364 and phagocytosed more avidly. Given that there are *PDR6* homologs in other fungal pathogens, it would
365 be interesting to see if this function is conserved. Notably, *PDR6* is missing in *C. deneoformans*, but present
366 in *C. gattii*. *C. deneoformans* is considerably less pathogenic than *C. neoformans,* and *C. gattii* is considered
367 a primary pathogen, although is more associated with pneumonia than CNS infection. Would absence of
368 *PDR6* in *C. deneoformans* contribute to the virulence differences? Moreover, in addition to *PDR6*, *C.*
369 *neoformans* has two additional half-size PDR transporters, which are missing in *C. gattii*. These are not in
370 clade VIb, but their function is nevertheless unknown. Elucidation of the diverse functions of ABC
371 transporters, specifically the PDR-type, has the potential to open new lines of investigation for better
372 treatments for this devastating disease.

373

374 **MATERIALS & METHODS**

375 **Strains, cell lines, growth conditions, and reagents**

376 Strains used were *C. neoformans* serotype A strain H99α and deletions in this background. H99α *afr1*Δ
377 and H99α *afr1*Δ/*afr2*Δ/*mdr1*Δ were a generous gift from Yun Chang (National Institutes of Health). The *S.*
378 *cerevisiae* strain ADΔΔ and the plasmids pABC3 and pABC3-KLmGH were graciously shared by Richard
379 Cannon (Otago University, New Zealand). Maintenance and growth conditions, as well as media details
380 can be found in Supplemental Text S1.

381 The human monocyte cell line THP-1 (ATCC TIB-202) was grown in THP-1 complete media and
382 differentiated with phorbol 12-myristate 12-acetate (PMA, Sigma) as described in (47). THP-1 cells were
383 split every 3-4 days and new vials were thawed every month. Details on complete media preparation and
384 differentiation into macrophages can be found in Supplemental Text S1.
385 All antifungals, xenobiotics, and other chemicals used were obtained through VWR or from Sigma.
386 Details on the preparation of stock solutions, including solvent concentrations, as well as their storage
387 information can be found in Supplemental Text S1.
388

389 **Fungal genome manipulation**

390 Since complementation strains of the original *pdr6*Δ proved challenging to create, we used the split
391 marker method (48) to delete *PDR6* (CNAG_06909) in H99α after amplifying NAT resistance split marker
392 fragments from genomic DNA of strain 1F1 (*pdr6*Δ) from the Madhani deletion collection. Three
393 independent *pdr6*Δ mutant strains were generated to verify that all observed phenotypes are a direct
394 result of the loss of *PDR6* (Fig. S2). Additionally, we performed whole genome sequencing on the
395 generated *pdr6*Δ mutants to confirm proper genetic manipulation (data not shown).
396

397 **Drug susceptibility assays**

398 The CLSI M27-A3 reference method was used to determine the MIC of each drug (49). Briefly, the
399 compounds to be tested were prepared at 2X the final concentration from stock solutions in RPMI 1640
400 medium. These were dispensed in a 96-well plate with 2-fold serial dilutions. 500 cells were then added
401 to each well. Plates were incubated at 37°C + 5% CO_2 for 48 – 72 hr. Minimal inhibitory concentrations
402 (MICs) were quantified by measuring the OD_{600} using a microtiter plate reader. For details on the
403 compounds and concentration ranges tested see Supplemental Text S1.

404 The MIC of FLC was also determined on RPMI plates with Epsilometer test strips (Etest strips;
405 Liofilchem Thermo). Approximately 5 X 10^4 cells were plated on RPMI agar plates before application of
406 the Etest strips. Plates were incubated at 30°C for 48 hr.
407

408 **Checkerboard assays**

409 Checkerboard assays to assess the fractional inhibitory concentrations (FICs) for combinations of
410 antifungal drugs was performed as previously described (50). Log-phase cultures were used and mixed
411 with the antifungal stocks in RPMI 1640. For more details on the procedure, final antifungal
412 concentrations, and calculations of the FIC index, see Supplemental Text S1. A FIC index value of ≤ 0.5 is
413 considered synergistic, additive if the value is between 1.0 and 0.5, and antagonistic if the FIC index is ≥
414 2.0.
415

416 **Flow cytometry analysis of the efflux of R6G, Nile Red, and Probe 1**

417 Accumulation assays was performed as previously described (21, 29). Briefly, strains were grown
418 overnight in YPD at 30°C with shaking. Log-phase cultures were incubated with the fluorescent reporters
419 in PBS for 30 min at 30°C with shaking. The reactions were stopped by cooling on ice, and the mixture was
420 diluted 40-fold in cold 1X PBS. The accumulation was immediately assessed by flow cytometry. For details
421 on the concentration of the reporters, the lasers and filters used, and how the data was analyzed see
422 Supplemental Text S1. Synthesis of Probe 1 was done in the Mobashery lab following published methods
423 (29). For a detailed synthetic scheme and characterization of the product see Supplemental Text S1.
424

425 **Liquid Chromatography/Mass Spectrometry (LC/MS)**

426 Log-phase cultures were incubated with FLC as above. A total of 200 µL was removed for CFU
427 quantification and the rest was processed to make the lysate. The lysate was mixed with same volume of

428 cold MeOH, vortexed, and spun down. The supernatant was mixed with the same volume of CH_2Cl_2,
429 vortexed, and spun down. The organic (bottom) phase was transferred into a glass tube, the solvent was
430 evaporated and the residues was resuspended in MeOH. At this point the samples were further cleaned
431 by passing through a solid-phase extraction (SPE) column. The elutes from SPE were concentrated by
432 speedvac, reconstituted in 50:50 water:MeOH, and analyzed using LC/MS. For details on the
433 instrumentation, columns, buffers, flow rates, software, and mass-spec parameters see Supplemental
434 Text S1.
435

436 **Phenotyping**

437 Strains tested were grown overnight in YPD, diluted to an OD_{600} of 0.2, and grown for two doublings. The
438 cultures were diluted to 1 x 10^7 cells/mL and serially diluted (10-fold) and spotted (5 µL) onto YPD with 1
439 M NaCl, 0.005% SDS, 0.1% Congo Red, and 0.5 µg/mL caffeine. Plates were incubated at 30°C for 48 – 72
440 hr.
441

442 **Uptake Assay**

443 Uptake assays were performed as previously described (22). Briefly, differentiated THP-1 cells were
444 incubated with Lucifer Yellow-stained fungal cells that had been opsonized with 40% fresh human serum
445 obtained from healthy donors (approved by the UND IRB committee as a non-human subject research
446 procedure). Following a 1 hr incubation, the plates were washed using a microplate washer (405LS, Biotek,
447 Winooski, VT), fixed with 4% formaldehyde, and stained with DAPI (Sigma) and CellMask Deep Red
448 (Invitrogen). NaN_3 in PBS was added to the plates and images were obtained using a Zeiss Axio Observer
449 microscope, equipped with an automated stage. Each well was automatically imaged in a 3x3 grid and the
450 images were analyzed using a Cell Profiler pipeline to determine phagocytic index (PI) values. For more
451 details on these procedures, including the Cell Profiler pipeline, see Supplemental Text S1.

452

453 **Conditioned media**

454 Conditioned media (CM) was generated as previously described (51). Briefly, overnight cultures were
455 diluted to 1 X 10^5 cells/mL in RPMI 1640 media and incubated for 5 days at 30ºC. Cells were removed by
456 centrifugation and the supernatant was filtered through a 0.25-µm filter.

457

458 **Capsule induction**

459 Cells were grown overnight in YPD, washed with DMEM, and 1 X 10^6 cells/mL were added to 24-well tissue
460 culture plates. Plates were incubated at 37ºC + 5% CO_2 for 24 hr. Cell suspension was collected and
461 washed, India ink was added, and samples were visualized on a Zeiss microscope. Images were analyzed
462 with ImageJ (NIH) for capsule thickness.

463

464 **Capsule shedding assay**

465 Capsule shedding assays were performed as previously described (38, 39). Briefly, strains were grown
466 overnight in YPD at 30ºC, washed, and diluted to 1 X 10^6 cells/mL in DMEM. Following a 15 hr incubation
467 at 37ºC + 5% CO_2, the samples were heated to denature enzymes, centrifuged to separate cells and
468 supernatant, and then stored at 4ºC. The samples were loaded on a 0.6% certified megabase agarose (Bio-
469 Rad) gel and subjected to electrophoresis for 15 hr at 25 V. Gel contents were transferred to a positively
470 charged membrane using a standard Southern blot protocol with 10X SSC. Following overnight transfer,
471 the membrane was blocked for 48 hr in 1X TBS-5% milk and incubated for 1 hr in 1X TBST-1% milk with 1
472 µg/mL of anti-GXM monoclonal antibody. Membrane was rinsed three times in 1X TBST and incubated for
473 1 hr in 1X TBST-1% milk with Odyssey antibody at 1:10,000. Membrane was rinsed again three times in 1X
474 TBST and imaged on the Odyssey (Licor).

475

476 **Biofilm/Adherence assay**

477 Cryptococcal adherence assays were performed in nontreated 96-well plates (CLS3631, Corning). Briefly,
478 strains were grown overnight in YPD, diluted to 1 X 10^7 cells/mL in DMEM, and 100 µl of cell suspension
479 was seeded. Plates were incubated at 37ºC + 5% CO_2 for 72 hr, washed with PBS, fixed with 4%
480 formaldehyde, blocked with 1.5% BSA and 0.1% NaN_3 in PBS, and incubated with anti-GXM primary and
481 secondary antibodies. Plates were imaged on the Odyssey and quantified using ImageStudio software.
482 Biofilms were also quantified by the XTT reduction assay, as previously described (52, 53). For details on
483 this assay see Supplemental Text S1.

484

485 **Filipin staining**

486 Staining of membrane sterols was performed as previously described (31, 54). Briefly, log-phase cultures
487 grown in YPD were stained for 5 min with 5 µg/mL of filipin (Sigma) and washed with PBS. After washing
488 cells were immediately visualized with an inverted Zeiss microscope. Fluorescence was calculated using
489 Cell Profiler software. Additionally, fluorescent levels were quantified with a fluorescent plate reader (Bio-
490 Tek). Fluorescence was measured at the range of 360 to 470 nm wavelength and normalized by OD_{600}.

491

492 **Mouse virulence studies**

493 To test virulence in a murine model, strains were cultured overnight in YPD, collected, washed, and diluted
494 to 10^6 cells/mL in DPBS. 50 µL of the cell suspension (or DPBS for the mock-infected) was used to
495 intranasally inoculate groups of five mice (5 to 6-week-old female A/Jcr mice; Jackson Laboratories).
496 Animals were closely monitored and sacrificed if they lost >20% relative to peak weight or at the end of
497 the experiment (41 days). Homogenates of lungs, brains, and spleens were plated to determine organ
498 burden.

499

500 **ACKNOWLEDGMENTS**

501 We acknowledge assistance and support for the LC-MS/MS by Dr. Mijoon Lee at the Notre Dame Mass
502 Spectrometry Core. We thank Dr. Richard Cannon for their gift of the ADΔΔ strain and associated
503 plasmids. We acknowledge financial support from the Warren Center for Drug Discovery for a Sean
504 Cocchia Rare Disease Research seed grant. We also thank members of the Santiago-Tirado lab for
505 thoughtful comments and feedback on this work.

506

507 **REFERENCES**

508 1. Higgins CF. 2001. ABC transporters: physiology, structure and mechanism--an overview. Res
509 Microbiol 152:205-10.
510 2. Jungwirth H, Kuchler K. 2006. Yeast ABC transporters-- a tale of sex, stress, drugs and aging.
511 FEBS Lett 580:1131-8.
512 3. Holland IB, Cole SPC, Kuchler K, Higgins CF. 2003. ABC Proteins from bacteria to man
513 doi:https://doi.org/10.1016/B978-0-12-352551-2.X5000-8. Academic Press, Amsterdam.
514 4. Khunweeraphong N, Kuchler K. 2021. Multidrug Resistance in Mammals and Fungi-From MDR to
515 PDR: A Rocky Road from Atomic Structures to Transport Mechanisms. Int J Mol Sci 22.
516 5. Lamping E, Baret PV, Holmes AR, Monk BC, Goffeau A, Cannon RD. 2010. Fungal PDR
517 transporters: Phylogeny, topology, motifs and function. Fungal Genet Biol 47:127-42.
518 6. Bongomin F, Gago S, Oladele RO, Denning DW. 2017. Global and Multi-National Prevalence of
519 Fungal Diseases-Estimate Precision. J Fungi (Basel) 3.
520 7. Niimi M, Tanabe K, Wada S, Yamazaki A, Uehara Y, Niimi K, Lamping E, Holmes AR, Monk BC,
521 Cannon RD. 2005. [ABC transporters of pathogenic fungi: recent advances in functional
522 analyses]. Nihon Ishinkin Gakkai Zasshi 46:249-60.
523 8. May RC, Stone NR, Wiesner DL, Bicanic T, Nielsen K. 2016. Cryptococcus: from environmental
524 saprophyte to global pathogen. Nat Rev Microbiol 14:106-17.
525 9. Rajasingham R, Smith RM, Park BJ, Jarvis JN, Govender NP, Chiller TM, Denning DW, Loyse A,
526 Boulware DR. 2017. Global burden of disease of HIV-associated cryptococcal meningitis: an
527 updated analysis. Lancet Infect Dis 17:873-881.
528 10. Coelho C, Casadevall A. 2016. Cryptococcal therapies and drug targets: the old, the new and the
529 promising. Cell Microbiol 18:792-9.
530 11. Zhang J, Li L, Lv Q, Yan L, Wang Y, Jiang Y. 2019. The Fungal CYP51s: Their Functions, Structures,
531 Related Drug Resistance, and Inhibitors. Front Microbiol 10:691.
532 12. Bongomin F, Oladele RO, Gago S, Moore CB, Richardson MD. 2018. A systematic review of
533 fluconazole resistance in clinical isolates of Cryptococcus species. Mycoses 61:290-297.
534 13. Rothe C, Sloan DJ, Goodson P, Chikafa J, Mukaka M, Denis B, Harrison T, van Oosterhout JJ,
535 Heyderman RS, Lalloo DG, Allain T, Feasey NA. 2013. A prospective longitudinal study of the
536 clinical outcomes from cryptococcal meningitis following treatment induction with 800 mg oral
537 fluconazole in Blantyre, Malawi. PLoS One 8:e67311.
538 14. Sionov E, Chang YC, Garraffo HM, Dolan MA, Ghannoum MA, Kwon-Chung KJ. 2012.
539 Identification of a Cryptococcus neoformans cytochrome P450 lanosterol 14alpha-demethylase

540 (Erg11) residue critical for differential susceptibility between fluconazole/voriconazole and
541 itraconazole/posaconazole. Antimicrob Agents Chemother 56:1162-9.
542 15. Rodero L, Mellado E, Rodriguez AC, Salve A, Guelfand L, Cahn P, Cuenca-Estrella M, Davel G,
543 Rodriguez-Tudela JL. 2003. G484S amino acid substitution in lanosterol 14-alpha demethylase
544 (ERG11) is related to fluconazole resistance in a recurrent Cryptococcus neoformans clinical
545 isolate. Antimicrob Agents Chemother 47:3653-6.
546 16. Bennett RJ, Forche A, Berman J. 2014. Rapid mechanisms for generating genome diversity:
547 whole ploidy shifts, aneuploidy, and loss of heterozygosity. Cold Spring Harb Perspect Med 4.
548 17. Stone NR, Rhodes J, Fisher MC, Mfinanga S, Kivuyo S, Rugemalila J, Segal ES, Needleman L,
549 Molloy SF, Kwon-Chung J, Harrison TS, Hope W, Berman J, Bicanic T. 2019. Dynamic ploidy
550 changes drive fluconazole resistance in human cryptococcal meningitis. J Clin Invest 129:999-
551 1014.
552 18. Holmes AR, Cardno TS, Strouse JJ, Ivnitski-Steele I, Keniya MV, Lackovic K, Monk BC, Sklar LA,
553 Cannon RD. 2016. Targeting efflux pumps to overcome antifungal drug resistance. Future Med
554 Chem 8:1485-501.
555 19. Posteraro B, Sanguinetti M, Sanglard D, La Sorda M, Boccia S, Romano L, Morace G, Fadda G.
556 2003. Identification and characterization of a Cryptococcus neoformans ATP binding cassette
557 (ABC) transporter-encoding gene, CnAFR1, involved in the resistance to fluconazole. Mol
558 Microbiol 47:357-71.
559 20. Sanguinetti M, Posteraro B, La Sorda M, Torelli R, Fiori B, Santangelo R, Delogu G, Fadda G.
560 2006. Role of AFR1, an ABC transporter-encoding gene, in the in vivo response to fluconazole
561 and virulence of Cryptococcus neoformans. Infect Immun 74:1352-9.
562 21. Chang M, Sionov E, Khanal Lamichhane A, Kwon-Chung KJ, Chang YC. 2018. Roles of Three
563 Cryptococcus neoformans and Cryptococcus gattii Efflux Pump-Coding Genes in Response to
564 Drug Treatment. Antimicrob Agents Chemother 62.
565 22. Santiago-Tirado FH, Peng T, Yang M, Hang HC, Doering TL. 2015. A Single Protein S-acyl
566 Transferase Acts through Diverse Substrates to Determine Cryptococcal Morphology, Stress
567 Tolerance, and Pathogenic Outcome. PLoS Pathog 11:e1004908.
568 23. Velamakanni S, Wei SL, Janvilisri T, van Veen HW. 2007. ABCG transporters: structure, substrate
569 specificities and physiological roles : a brief overview. J Bioenerg Biomembr 39:465-71.
570 24. Kovalchuk A, Driessen AJ. 2010. Phylogenetic analysis of fungal ABC transporters. BMC
571 Genomics 11:177.
572 25. Oliveira FFM, Paes HC, Peconick LDF, Fonseca FL, Marina CLF, Bocca AL, Homem-de-Mello M,
573 Rodrigues ML, Albuquerque P, Nicola AM, Alspaugh JA, Felipe MSS, Fernandes L. 2020. Erg6
574 affects membrane composition and virulence of the human fungal pathogen Cryptococcus
575 neoformans. Fungal Genet Biol 140:103368.
576 26. Brown HE, Telzrow CL, Saelens JW, Fernandes L, Alspaugh JA. 2020. Sterol-Response Pathways
577 Mediate Alkaline Survival in Diverse Fungi. mBio 11.
578 27. Kolaczkowski M, van der Rest M, Cybularz-Kolaczkowska A, Soumillion JP, Konings WN, Goffeau
579 A. 1996. Anticancer drugs, ionophoric peptides, and steroids as substrates of the yeast
580 multidrug transporter Pdr5p. J Biol Chem 271:31543-8.
581 28. Ivnitski-Steele I, Holmes AR, Lamping E, Monk BC, Cannon RD, Sklar LA. 2009. Identification of
582 Nile red as a fluorescent substrate of the Candida albicans ATP-binding cassette transporters
583 Cdr1p and Cdr2p and the major facilitator superfamily transporter Mdr1p. Anal Biochem 394:87-
584 91.
585 29. Benhamou RI, Bibi M, Steinbuch KB, Engel H, Levin M, Roichman Y, Berman J, Fridman M. 2017.
586 Real-Time Imaging of the Azole Class of Antifungal Drugs in Live Candida Cells. ACS Chem Biol
587 12:1769-1777.

588 30. Paul S, Kannan I, Mohanram K. 2019. Extensive ERG11 mutations associated with fluconazole-
589 resistant Candida albicans isolated from HIV-infected patients. Curr Med Mycol 5:1-6.
590 31. Altamirano S, Simmons C, Kozubowski L. 2018. Colony and Single Cell Level Analysis of the
591 Heterogeneous Response of Cryptococcus neoformans to Fluconazole. Front Cell Infect
592 Microbiol 8:203.
593 32. Godinho CP, Prata CS, Pinto SN, Cardoso C, Bandarra NM, Fernandes F, Sa-Correia I. 2018. Pdr18
594 is involved in yeast response to acetic acid stress counteracting the decrease of plasma
595 membrane ergosterol content and order. Sci Rep 8:7860.
596 33. Godinho CP, Costa R, Sa-Correia I. 2021. The ABC transporter Pdr18 is required for yeast
597 thermotolerance due to its role in ergosterol transport and plasma membrane properties.
598 Environ Microbiol 23:69-80.
599 34. Lamping E, Monk BC, Niimi K, Holmes AR, Tsao S, Tanabe K, Niimi M, Uehara Y, Cannon RD.
600 2007. Characterization of three classes of membrane proteins involved in fungal azole resistance
601 by functional hyperexpression in Saccharomyces cerevisiae. Eukaryot Cell 6:1150-65.
602 35. Madani G, Lamping E, Lee HJ, Niimi M, Mitra AK, Cannon RD. 2021. Small-Scale Plasma
603 Membrane Preparation for the Analysis of Candida albicans Cdr1-mGFPHis. J Vis Exp
604 doi:10.3791/62592.
605 36. Gaylord EA, Choy HL, Doering TL. 2020. Dangerous Liaisons: Interactions of Cryptococcus
606 neoformans with Host Phagocytes. Pathogens 9.
607 37. Zaragoza O, Rodrigues ML, De Jesus M, Frases S, Dadachova E, Casadevall A. 2009. The capsule
608 of the fungal pathogen Cryptococcus neoformans. Adv Appl Microbiol 68:133-216.
609 38. Denham ST, Verma S, Reynolds RC, Worne CL, Daugherty JM, Lane TE, Brown JCS. 2018.
610 Regulated Release of Cryptococcal Polysaccharide Drives Virulence and Suppresses Immune Cell
611 Infiltration into the Central Nervous System. Infect Immun 86.
612 39. Yoneda A, Doering TL. 2008. Regulation of Cryptococcus neoformans capsule size is mediated at
613 the polymer level. Eukaryot Cell 7:546-9.
614 40. Martinez LR, Casadevall A. 2015. Biofilm Formation by Cryptococcus neoformans. Microbiol
615 Spectr 3.
616 41. Lee HH, Del Pozzo J, Salamanca SA, Hernandez H, Martinez LR. 2019. Reduced phagocytosis and
617 killing of Cryptococcus neoformans biofilm-derived cells by J774.16 macrophages is associated
618 with fungal capsular production and surface modification. Fungal Genet Biol 132:103258.
619 42. Ravi S, Pierce C, Witt C, Wormley FL, Jr. 2009. Biofilm formation by Cryptococcus neoformans
620 under distinct environmental conditions. Mycopathologia 167:307-14.
621 43. Jorda T, Puig S. 2020. Regulation of Ergosterol Biosynthesis in Saccharomyces cerevisiae. Genes
622 (Basel) 11.
623 44. Baumann NA, Sullivan DP, Ohvo-Rekila H, Simonot C, Pottekat A, Klaassen Z, Beh CT, Menon AK.
624 2005. Transport of newly synthesized sterol to the sterol-enriched plasma membrane occurs via
625 nonvesicular equilibration. Biochemistry 44:5816-26.
626 45. Kerr ID, Hutchison E, Gerard L, Aleidi SM, Gelissen IC. 2021. Mammalian ABCG-transporters,
627 sterols and lipids: To bind perchance to transport? Biochim Biophys Acta Mol Cell Biol Lipids
628 1866:158860.
629 46. Santiago-Tirado FH, Doering TL. 2017. False friends: Phagocytes as Trojan horses in microbial
630 brain infections. PLoS Pathog 13:e1006680.
631 47. Liu OW, Chun CD, Chow ED, Chen C, Madhani HD, Noble SM. 2008. Systematic genetic analysis
632 of virulence in the human fungal pathogen Cryptococcus neoformans. Cell 135:174-88.
633 48. Fu J, Hettler E, Wickes BL. 2006. Split marker transformation increases homologous integration
634 frequency in Cryptococcus neoformans. Fungal Genet Biol 43:200-12.

635 49. CLSI. 2017. Reference Method for Broth Dilution Antifungal Susceptibility Testing of Yeasts. 4th
636 ed. CLSI Standard M27. Clinical and Laboratory Standard Institute, Wayne, PA.
637 50. Franzot SP, Casadevall A. 1997. Pneumocandin L-743,872 enhances the activities of
638 amphotericin B and fluconazole against Cryptococcus neoformans in vitro. Antimicrob Agents
639 Chemother 41:331-6.
640 51. Albuquerque P, Nicola AM, Nieves E, Paes HC, Williamson PR, Silva-Pereira I, Casadevall A. 2013.
641 Quorum sensing-mediated, cell density-dependent regulation of growth and virulence in
642 Cryptococcus neoformans. mBio 5:e00986-13.
643 52. Pierce CG, Uppuluri P, Tristan AR, Wormley FL, Jr., Mowat E, Ramage G, Lopez-Ribot JL. 2008. A
644 simple and reproducible 96-well plate-based method for the formation of fungal biofilms and its
645 application to antifungal susceptibility testing. Nat Protoc 3:1494-500.
646 53. Martinez LR, Casadevall A. 2005. Specific antibody can prevent fungal biofilm formation and this
647 effect correlates with protective efficacy. Infect Immun 73:6350-62.
648 54. Bang S, Kwon H, Hwang HS, Park KD, Kim SU, Bahn YS. 2014. 9-O-butyl-13-(4-
649 isopropylbenzyl)berberine, KR-72, is a potent antifungal agent that inhibits the growth of
650 Cryptococcus neoformans by regulating gene expression. PLoS One 9:e109863.

651

652

653

654

655

656

657

658

659

660

661

662

663

664

665

666

667

668

669 **FIGURES AND FIGURE LEGENDS**

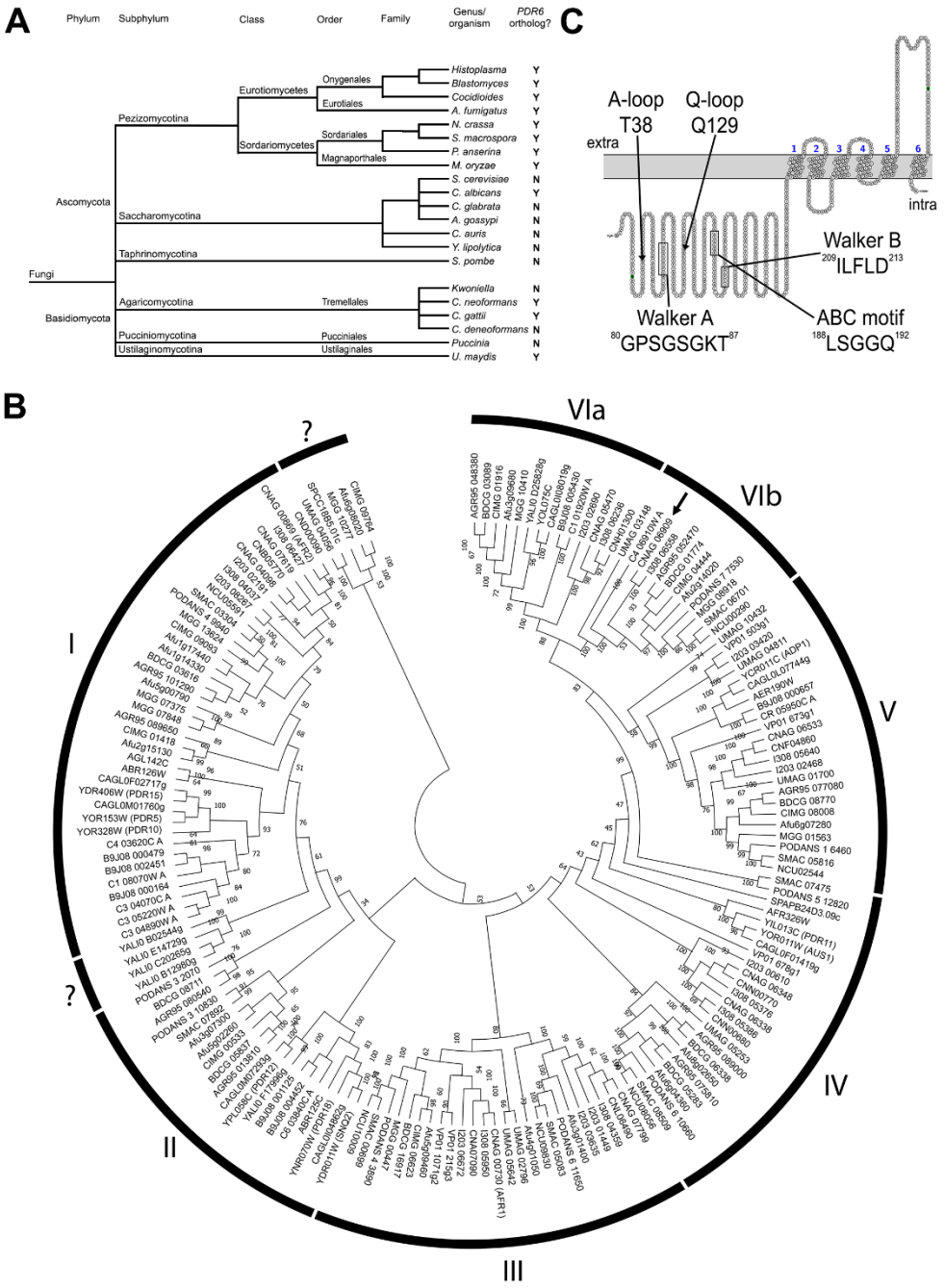

670

671 **FIG 1** *PDR6* contains all the features of a PDR-type ABC transporter and is conserved in a subset of fungal

672 pathogens. (A) Cladogram showing the fungal distribution of *PDR6* orthologs in the two main phyla. (B)

673 Global phylogenetic tree showing the evolutionary relationships of PDR-type ABC transporters in 21 fungal

674 organisms. Gene names are given in NCBI nomenclature. Tree was generated by Maximum Likelihood

675 Method using MEGA-X and confidence values determined from 500 bootstraps with bootstrap scores
676 shown at all nodes. The tree shown is the bootstrap consensus tree. Analysis reveals VI major clades with
677 *C. neoformans PDR6* housed in clade VIb. Arrow denotes location of *PDR6.* (C) Topology prediction of Pdr6
678 protein by Computational Analysis of the Membrane Protein Space (CAMPS) software showing the
679 domain arrangement of the half-size PDR transporter. The 5 main consensus motifs of the nucleotide
680 binding domain (NBD) are depicted.
681
682
683
684
685
686
687
688

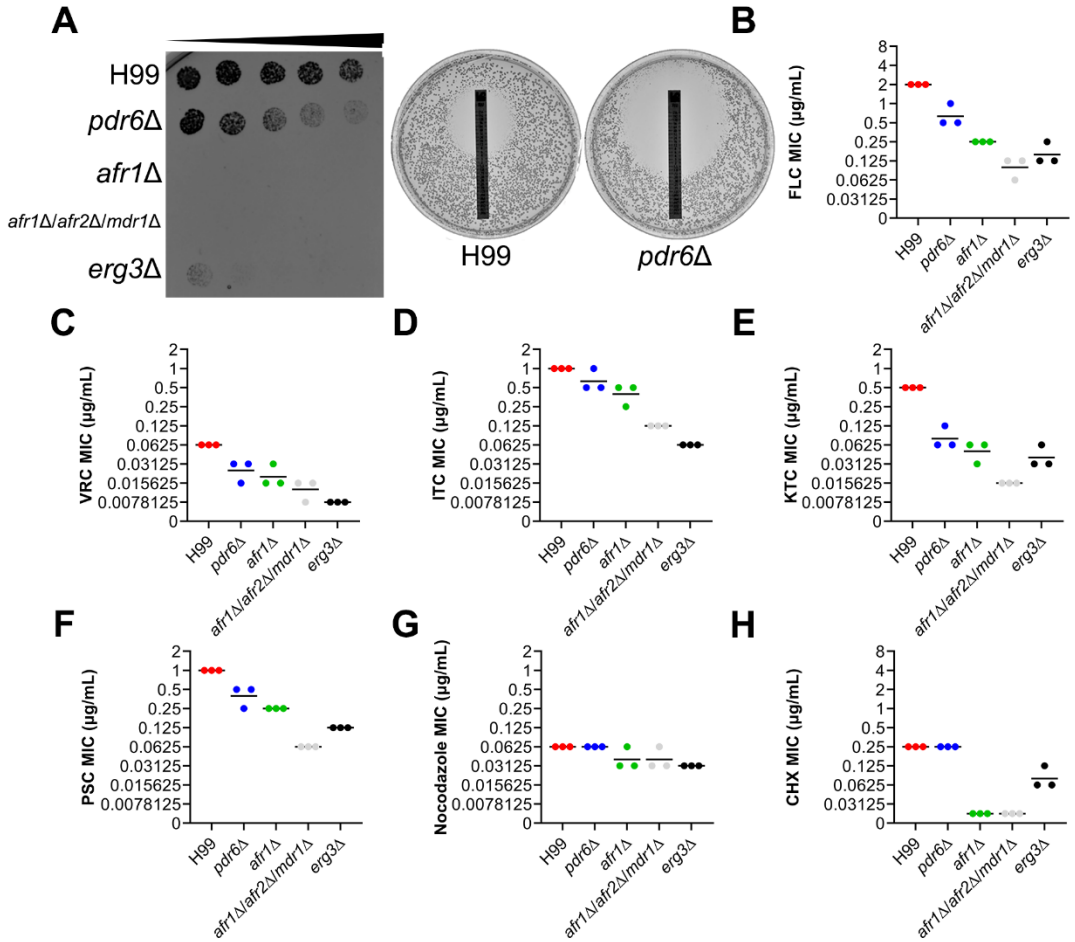

FIG 2 *PDR6* is involved in azole resistance. (A) The *pdr6*Δ mutant shows increased sensitivity to FLC gradient plates and Etest strips. (Left) 500 cells of the indicated strains were spotted across RPMI-1640 slant plate with peak FLC concentration of 4 µg/mL at the right side of the plate. (Right) FLC Etest strips were applied to RPMI-1640 plates with 2 x 10^5 cells of indicated strain. The MICs of the H99 and *pdr6*Δ mutant were 6 and 0.38 µg/mL, respectively. These plates were incubated for 72 hr at 30°C. (B-H) Quantitative broth microdilution assays were used to compare MICs of several antifungal compounds in the WT and *pdr6*Δ mutant. The CLSI M27-A3 reference method was repeated three times for each compound and the bars represent the average of the MICs. The details for each strain's MICs are listed in Table 1. FLC, fluconazole; VRC, voriconazole; ITC, itraconazole; KTC, ketoconazole; PSC, posaconazole; CHX, cycloheximide.

	MICs (µg/mL)													
Strain	**FLC**	**ITC**	**VRC**	**KTC**	**PSC**	**AMB**	**5-FC**	**CHX**	**Nocodazole**	**BER**	**PQ**	**TSA**	**Menadione (µM)**	**CSF**
H99	2	1	0.0625	0.5	1	4	2	0.25	0.0625	8	12.5	2	16	32
*pdr6*Δ	0.5	0.5	0.015625	0.0625	0.25	4	4	0.25	0.0625	8	12.5	2	16	64
*afr1*Δ	0.25	0.5	0.03125	0.0625	0.25	4	2	0.015625	0.0625	8	12.5	0.5	16	64
*afr1*Δ /*afr2*Δ /*mdr1*Δ	0.125	0.125	0.015625	0.015625	0.0625	4	4	0.015625	0.0625	8	12.5	0.5	8	64
*erg3*Δ	0.125	0.25	0.0078125	0.03125	0.125	4	2	0.0625	0.03125	0.5	3.125	0.5	16	32

Table 1 MICs of antifungals and xenobiotics. Values are representative of three biological replicates. FLC, fluconazole; ITC, itraconazole, KTC, ketoconazole; PSC, posaconazole; AMB, amphotericin B; 5-FC, 5-fluorocytosine; CHX, cycloheximide; BER, berberine; PQ, paraquat; TSA, trichostatin A; CSF, caspofungin.

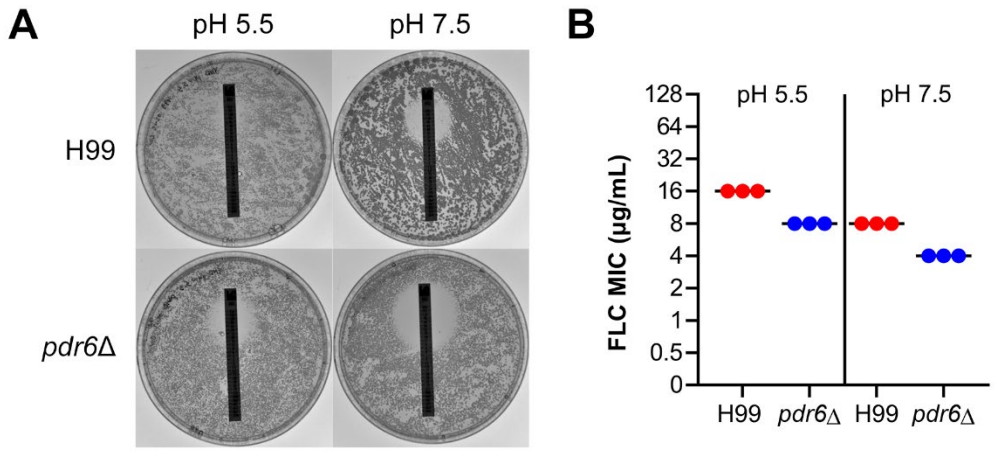

FIG S1 FLC hypersensitivity in *pdr6*Δ mutant is pH-independent. (A) Plates with FLC Etest strips to assess the zones of inhibition of H99 WT and *pdr6*Δ mutant cells grown on standard (pH 5.5) or alkaline (pH 7.5) YNB medium. Regardless of pH, the *pdr6*Δ mutant was 4X more susceptible than WT. The H99 and *pdr6*Δ mutant displayed FLC MICs of 64 and 16 µg/mL on the 5.5 pH plates and 24 and 6 µg/mL under alkaline conditions. Plates were imaged after 72 hr of growth at 30ºC. (B) MIC of FLC for H99 WT and *pdr6*Δ strains grown under alkaline conditions as determined by broth microdilution assays after 48 h of growth at 30ºC. Microdilution assays were repeated three times for each condition and black bars represent the average MIC respectively.

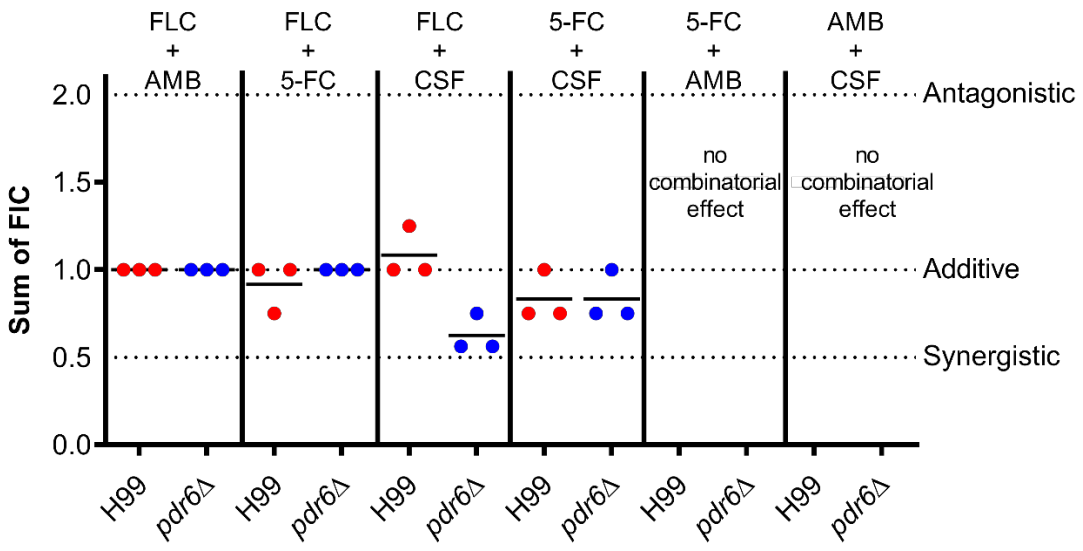

716

717 **FIG 3** Combinatorial FLC + CSF function synergistically in *pdr6*Δ mutant. Checkerboard assays assessed

718 changes in drug combinatorial activity in H99 and *pdr6*Δ strains. The combination of FLC + CSF resulted in

719 average sums of FIC of 1.083 and 0.625 in the H99 and *pdr6*Δ strain respectively. Calculations indicate a

720 change from additive to synergistic in the absence of *PDR6*. Checkerboard assays were repeated three

721 times for each combination and black bars represent the average sum of FIC.

722

723

724

725

726

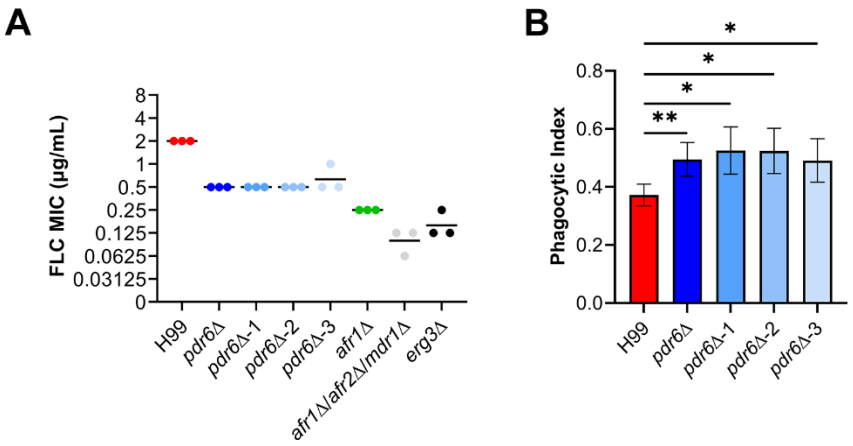

727

728 **FIG S2** Recreated *pdr6*Δ strains display identical phenotypes to original strain from deletion collection. (A)
729 Broth microdilution assays were used to compare FLC MICs of three independently recreated *pdr6*Δ
730 strains to the *pdr6*Δ strain from the deletion collection. Assay was repeated three times and black bars
731 represent the average MIC. (B) Comparative phagocytic indices of the library and recreated *pdr6*Δ mutants
732 with the H99 strain. All *pdr6*Δ strains displayed significantly higher phagocytic values than the WT. Values
733 represent the mean ± SD of a representative experiment from three biological replicates. Statistical
734 significance determined using one-way ANOVA with multiple comparisons (Welch's corrected), *P<0.05,
735 **P<0.01.

736

737

738

739

740

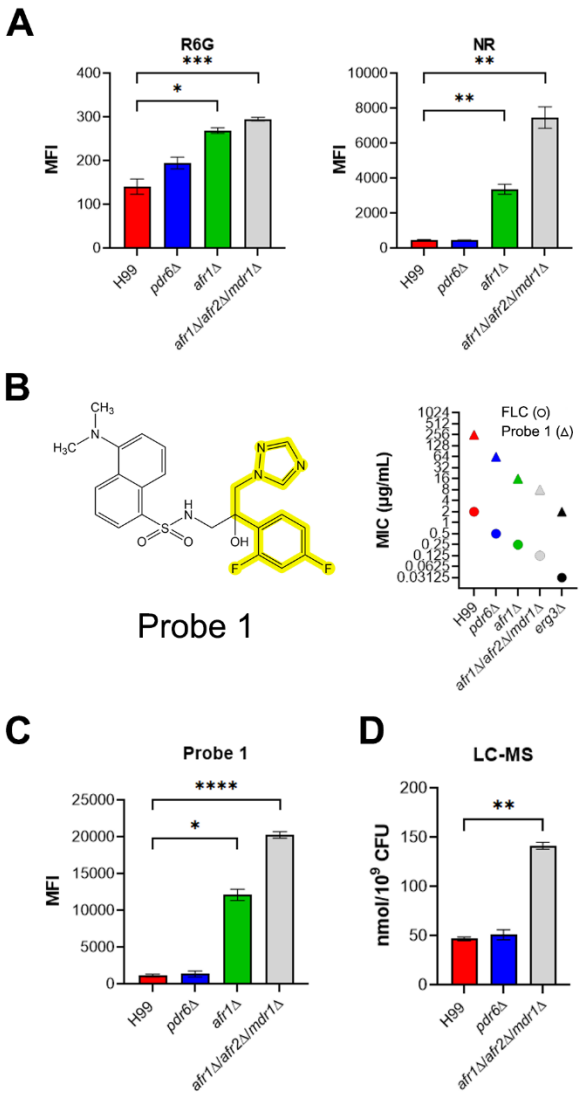

741

742 **FIG 4** Deletion of *PDR6* does not affect intracellular accumulation of fluorescent reporters. (A) H99 and
743 indicated deletion strains were incubated with 10 µM R6G or 7 µM NR for 30 min at 30ºC and the cells
744 were analyzed by flow cytometry. No significant difference in intracellular accumulation was observed
745 between the WT and *pdr6*Δ mutant. (B) (Left) Chemical structure of Probe 1 with FLC backbone
746 highlighted. (Right) Broth microdilution assays were performed to compare the MICs of FLC with Probe 1.
747 Regardless of strain, a 128-fold increase was observed in the MICs of Probe 1 when compared to FLC.
748 Microdilution assays were repeated three times and shown is a representative figure. (C) Indicated strains
749 were incubated with 10 µg/mL of Probe 1 as described above and accumulation assessed using flow

750 cytometry. (D) Accumulation of FLC was assessed in H99 and deletion strains using LC-MS/MS. Strains
751 were incubated with 16 µg/mL of FLC for 30 min at 30ºC. All values represent the mean ± SEM from three
752 to four independent experiments. Significance was determined using one-way ANOVA compared to H99
753 (Welch's corrected), *P<0.05, **P<0.01, ****P<0.0001.
754
755
756

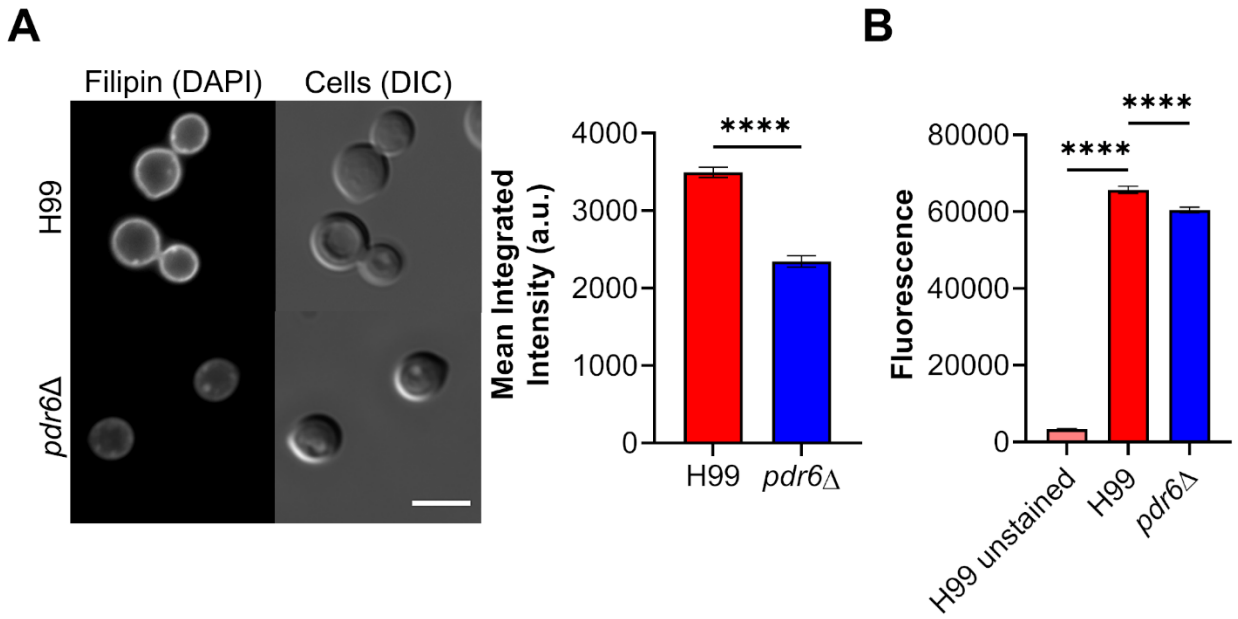

757
758 **FIG 5** *pdr6*Δ mutant displays reduced sterol content. (A) Filipin staining was used to assess sterol content
759 in WT and *pdr6*Δ strains. (Left) The *pdr6*Δ mutant displayed significantly less plasma membrane
760 fluorescence than the WT. Cells were incubated with 5 µg/mL for 5 min at 30ºC and visualized. Scale bar,
761 5 µm. (Right) Quantification of fluorescence was assessed using a Cell Profiler pipeline. Values represent
762 the mean ± SEM where n=50. Significance was determined using Student's T-test (Welch's corrected),
763 ****P<0.0001 (B) Total filipin staining was also measured using a fluorescent plate reader. Similarly, less
764 sterol was observed in the *pdr6*Δ strain when compared to the WT. Values represent the mean ± SEM

765 from three independent experiments. Significance was determined using one-way ANOVA with multiple

766 comparisons (Welch's corrected), ****P<0.0001.

767

768

769

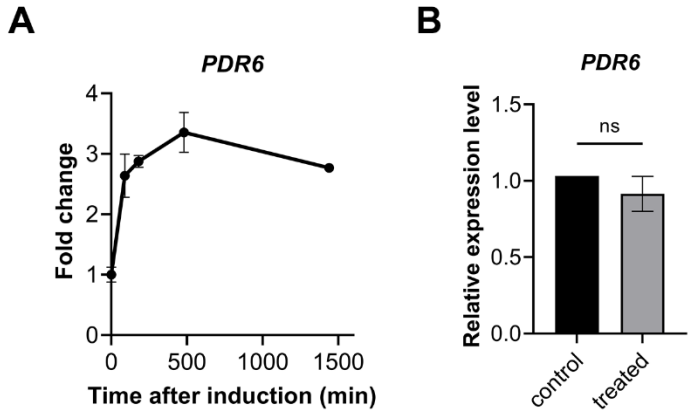

770

771 **FIG S3** *PDR6* is induced by host-like conditions. (A) Data from an RNA-seq experiment to analyze

772 expression levels of *PDR6* after shifting to host-like conditions. Expression increased about almost 3-fold

773 in the first 30 min and remained relatively high throughout 24 hr. (B) qRT-PCR measured transcript levels

774 of *PDR6* in response to FLC exposure. Log phase cells were either untreated (control) or treated with 4

775 µg/mL of FLC for 2 hr. No significant difference was observed in the presence of the antifungal. Expression

776 levels were normalized to that of the actin gene. Values represent the mean ± SEM of three biological

777 replicates.

778

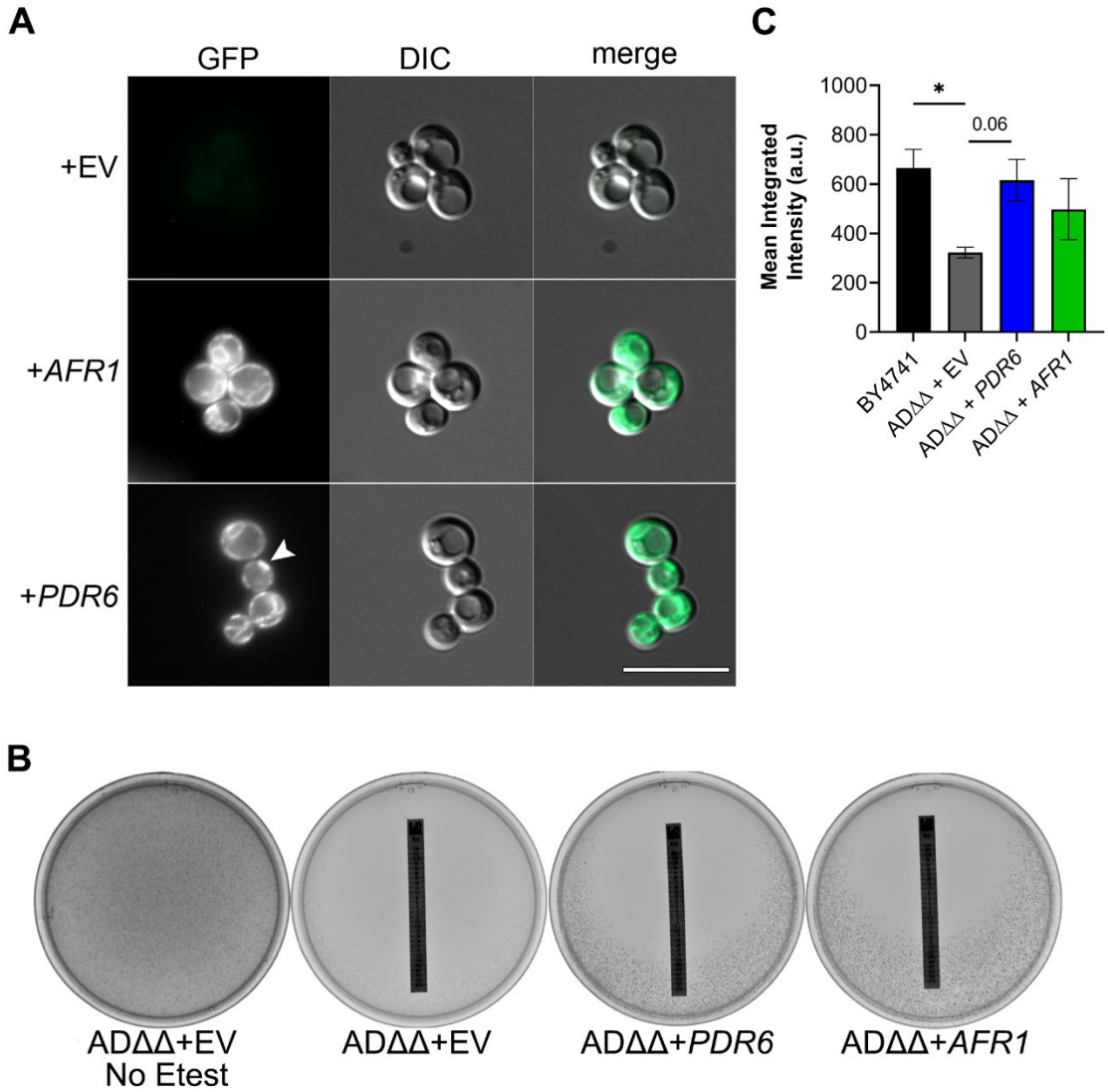

FIG 6 Pdr6 localizes to the ER and PM in *S. cerevisiae.* (A) Visualization of *S. cerevisiae* ADΔΔ expressing *C. neoformans PDR6* and *AFR1,* or empty vector. GFP-tagged proteins localization is consistent with the ER and PM. Representative images of transformed strains. Arrow denotes an enrichment of Pdr6-GFP on the PM. Scale bar, 10 μm. EV, empty vector. (B) Function of expressed cryptococcal proteins was assessed using FLC Etest strips. Both strains expressing *PDR6* (MIC = 0.25 μg/mL) and *AFR1* (MIC = 0.75 μg/mL) display increased resistance to FLC compared to empty vector control (MIC = 0.064 μg/mL) but the strain expressing *AFR1* was most resistant. Plates were incubated at 30°C for 96 hr and imaged. (C) Quantification of sterol content in transformed strains. The ADΔΔ + *PDR6* displays increased filipin staining

788 compared to the ADΔΔ control and ADΔΔ + *AFR1* but less than the WT BY4741 strain. Log-phase cells were

789 incubated with filipin as previously described and imaged. Values represent the mean ± SEM where n=50.

790 Significance was determined using one-way ANOVA (Brown-Forsythe and Welch's corrected), * $P < 0.05$.

791

792

793

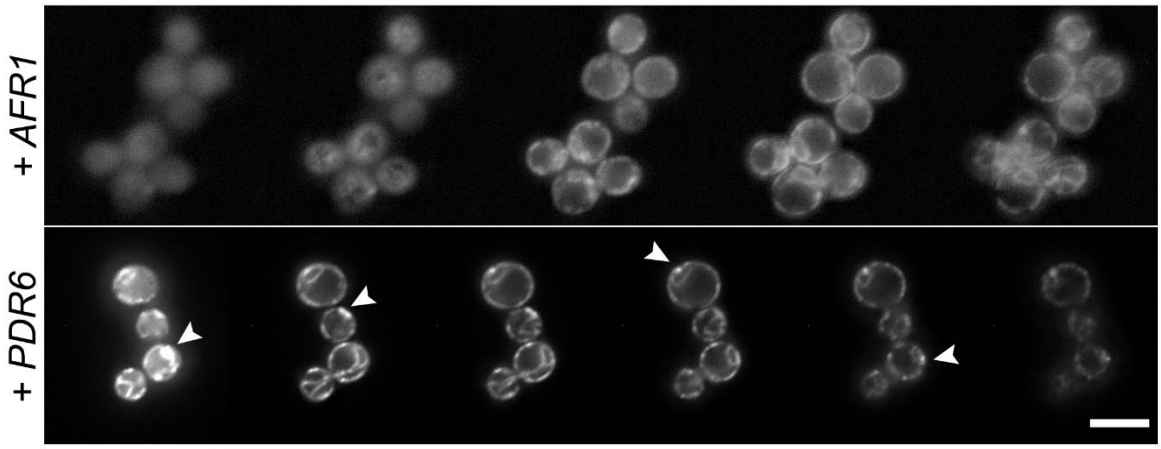

794

795 **FIG S4** Pdr6-GFP exhibits small areas of intense localization to membranes of the ER and PM (arrowheads).

796 These intense puncta are not seen in the Afr1-GFP cells. Scale bar is 5 μm.

797

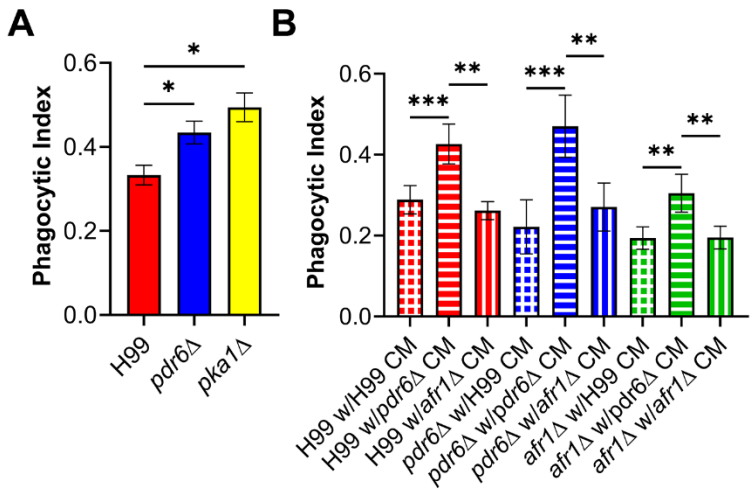

FIG 7 *pdr6*Δ mutant conditioned media (CM) increases the phagocytosis of H99 WT by host macrophages. (A) Uptake assays of WT and deletion strains were performed to determine phagocytic indices of respective strains. The *pdr6*Δ mutant displayed increased uptake compared to the H99 strain. The *pka1*Δ cells are used as a positive control. Stained and opsonized log-phase cells were incubated for 1 hr with THP-1 cells and imaged using automated microscopy. Values represent the mean ± SEM from three independent experiments. (B) Uptake assay using CM from cryptococcal strains was performed. CM obtained by centrifugation and filtration of supernatants from 5-day cultures incubated at 37°C + 5% CO_2 in RPMI-1640 media. The *pdr6*Δ CM altered the phagocytic uptake values of the WT strain and vice versa, whereas the *afr1*Δ CM has no effect. Values represent the mean ± SD from a representative experiment. Significance was determined using one-way ANOVA with multiple comparisons (Welch's corrected), *P<0.05; **P<0.01; ***P<0.001.

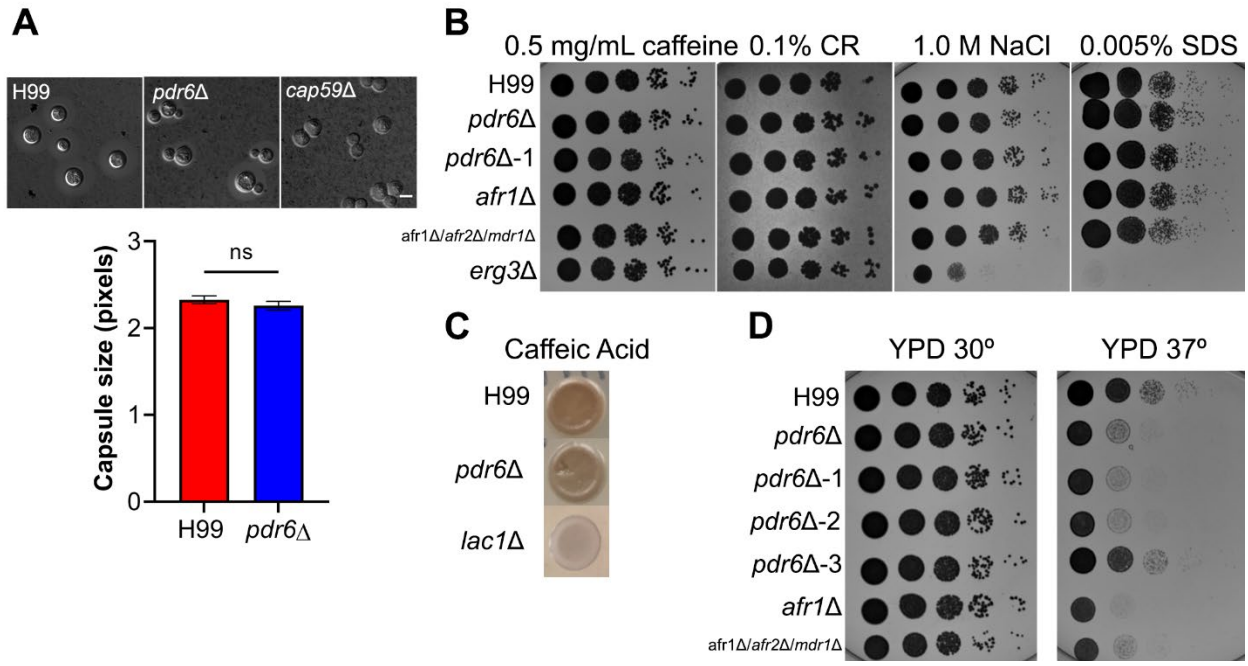

FIG S5 *pdr6*Δ mutant exhibits a mild defect in thermotolerance but behaves identical to H99 WT in other virulence factors and stress conditions. (A) Capsule induction assays were performed to determine capsule thickness in cryptococcal strains. Visualization and quantification of 24 hr cultures revealed that there was no significant difference in capsule size between the H99 and *pdr6*Δ mutant. Scale bar, 5 µm. Values represent the mean ± SEM where n=50. (B) Growth on stress plates was assessed to determine potential membrane or cell wall defects in the indicated cryptococcal strains. No differences were observed in the *pdr6*Δ mutant. Mid-log phase cultures were serially diluted on plates with cell wall/PM stressors and incubated for 72 hr at 30ºC. CR, Congo Red. (C) Melanization was assessed by pigmentation on caffeic acid plates. 5.0 x 10^3 cells were spotted and incubated as above. (D) Thermotolerance was assessed by spotting strains on YPD plates and incubating plates at 30ºC and 37ºC for 72 hr. A mild defect in growth was observed in the *pdr6*Δ mutant compared to the WT strain.

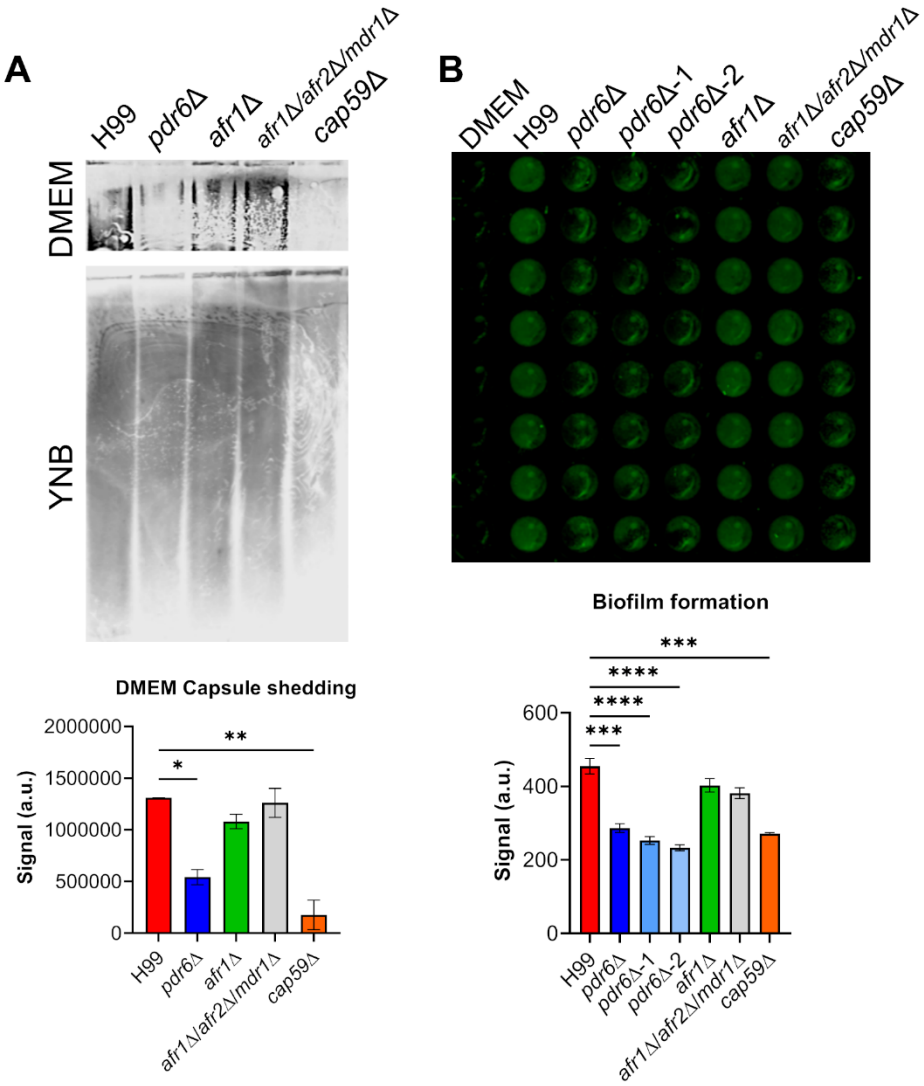

FIG 8 Deletion of *PDR6* alters capsular secretion and biofilm formation. (A) Capsule shedding assays were performed to determine amount of GXM secreted from cryptococcal strains. Visualization of released GXM was observed on immunoblot using fluorescent detection (Odyssey, LiCor). Quantification of signal revealed that the *pdr6*Δ mutant shed significantly less capsule than the WT strain. Values represent the mean ± SD from a representative experiment. Significance was determined using one-way ANOVA compared to H99 (Welch's corrected), *P<0.05; **P<0.01. (B) Biofilm forming assays were performed to again analyze shed capsule. Nontreated microtiter plates were incubated for 72 hr, washed, and visualized for biofilms using a fluorescent imaging system. (Odyssey, LiCor). Quantification of signal reveal that all

834 *pdr6*Δ mutants form weaker/less adherent biofilms when compared to the WT. Values represent the

835 mean ± SD from a representative experiment. Significance was determined using one-way ANOVA

836 compared to H99 (Welch's corrected), ***P<0.001; ****P<0.0001.

837

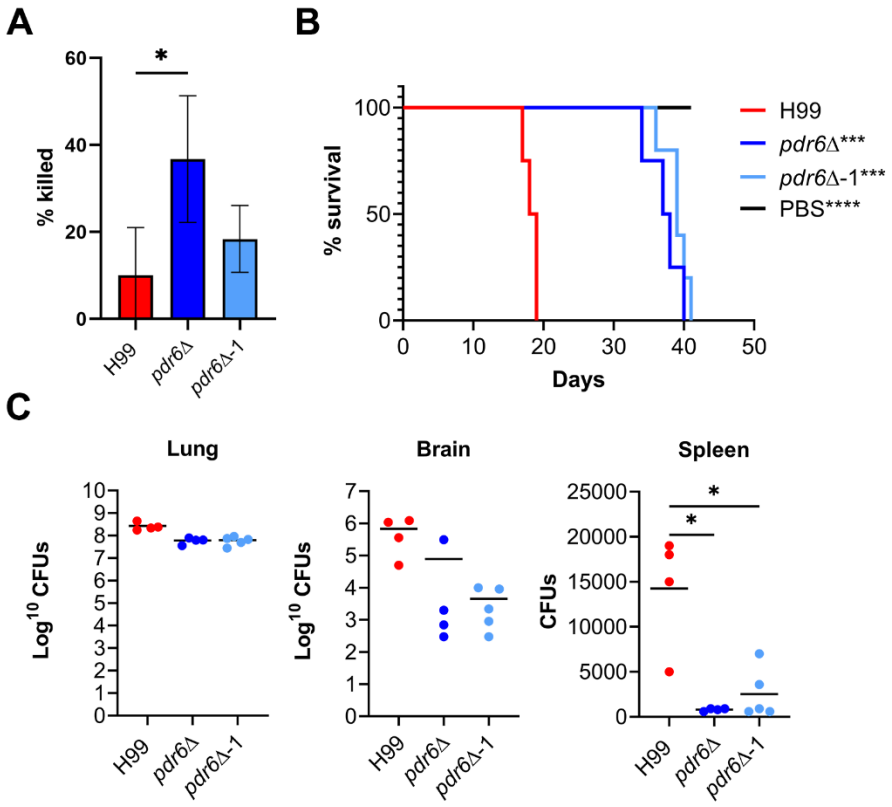

838

839 **FIG 9** *pdr6*Δ mutant displays attenuated virulence *in vitro* and *in vivo.* (A) *In vitro* survival of H99 and *pdr6*Δ

840 strains. Fungi and THP-1 cells were coincubated for 1 hr at an MOI of 0.1, washed to remove free

841 cryptococci, and half the samples lysed to determine intracellular fungi and the other half grown for an

842 additional 3 hr, after which they were also lysed. Shown in % killed, values represent the mean ± SEM

843 from three independent experiments. Significance was determined using one-way ANOVA compared to

844 H99 (Friedman corrected), *P<0.05. (B) *In vivo* survival curve of H99 and *pdr6*Δ-infected mice. 5 AJ/Cr mice

845 per group were infected intranasally with 5 x 10^4 *C. neoformans*, or mock infected with DPBS and

846 monitored for up to 41 days (experiment terminated when the last infected mouse died). Significance was

847 determined using Mantel-Cox test, ***P<0.001. (C) Calculated organ burden of H99 and *pdr6*Δ strains at
848 time of death. Organs were harvested, homogenized, and dilutions were plated on YPD. Plates were
849 incubated for 48 hr and CFUs counted. Each data point represents a mouse and black bars represent the
850 mean. Significance was determined using one-way ANOVA with multiple comparisons (Welch's
851 corrected), *P<0.05.
852

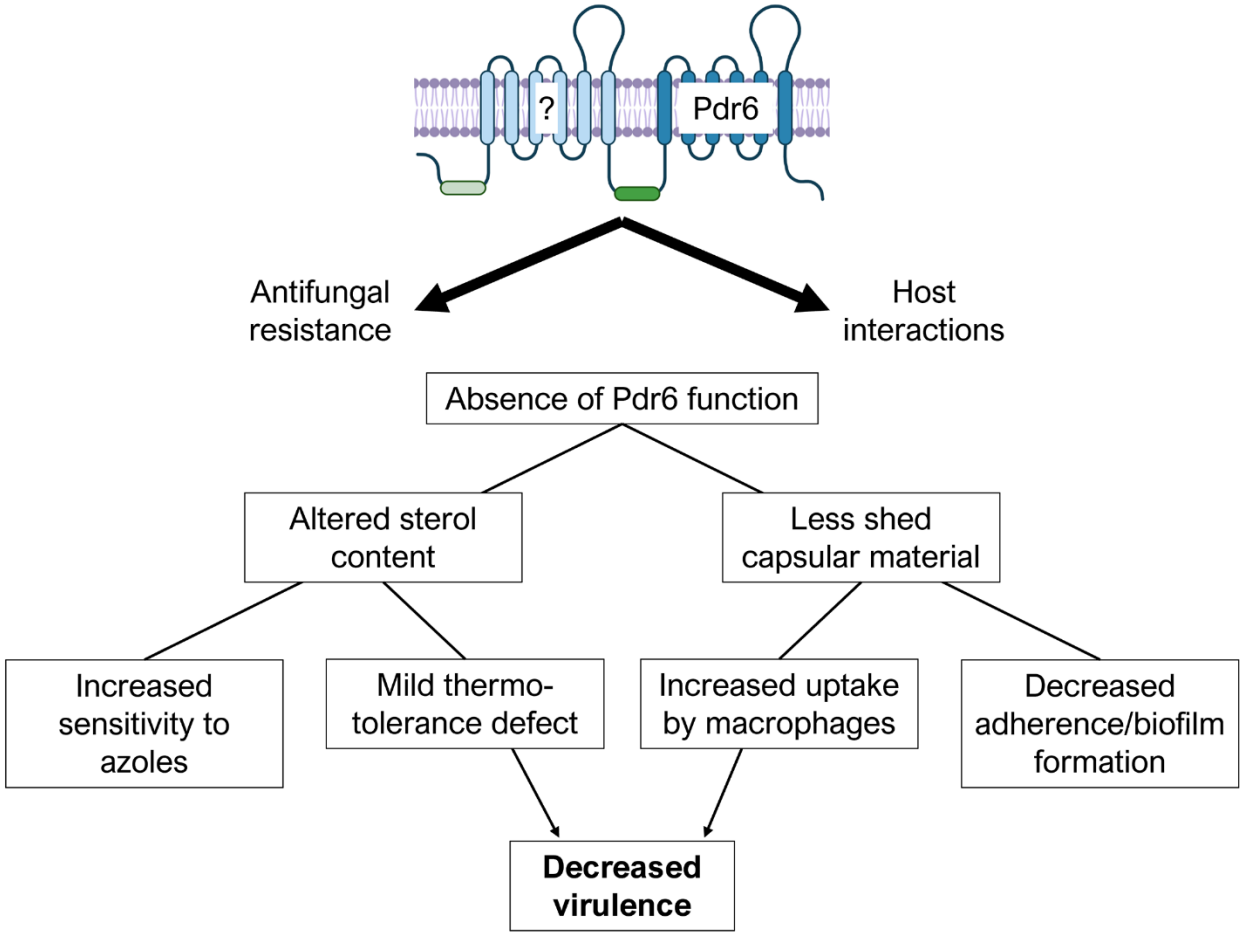

853
854 **FIG 10** Model of Pdr6 and relationship to antifungal resistance, host interactions, and virulence. Pdr6 is a
855 half-size transporter (dark blue), hence it needs to dimerize with itself or another half-size transporter
856 (light blue) to be functional.